



Generation and evolution of intense ion cyclotron turbulence by artificial plasma cloud in the magnetosphere

Gurudas Ganguli,¹ Leonid Rudakov,² Manish Mithaiwala,³ and Konstantinos Papadopoulos⁴

Received 6 November 2006; revised 29 January 2007; accepted 6 March 2007; published 16 June 2007.

[1] It is shown that intense ion cyclotron turbulence can be induced in the near-Earth space by shaped release of neutral gas of materials such as lithium, cesium, etc. Release of 1 ton of neutral lithium gas in the Earth's equatorial plane at $L = 2$ can introduce about 30 GJ of energy which can be used to excite waves around the lithium ion cyclotron harmonics that readily evolves into the turbulent state. The energy is obtained by converting the orbital kinetic energy of the neutral lithium atoms into free energy for the electromagnetic waves through photoionization and creation of a ring distribution in the lithium ion velocity perpendicular to the ambient magnetic field. This distribution function is highly unstable and can spontaneously trigger large amplitude shear Alfvén waves near lithium cyclotron harmonics with unique nonlinear properties. These waves lead to pitch angle scattering of the trapped electrons in a broad energy band.

Citation: Ganguli, G., L. Rudakov, M. Mithaiwala, and K. Papadopoulos (2007), Generation and evolution of intense ion cyclotron turbulence by artificial plasma cloud in the magnetosphere, *J. Geophys. Res.*, 112, A06231, doi:10.1029/2006JA012162.

1. Introduction

[2] Turbulence in a multispecies plasma is not only of interest to basic plasma physics but also has practical importance because it determines the general plasma state in space. It can affect the composition and dynamics of the plasma constituents and hence is a key factor in the determination of space weather which is critically important to the reliability of space assets. Consequently, low-frequency turbulence in space plasmas has been extensively studied [Onishchenko *et al.*, 2003; Voitenko and Goossens, 2005; Shukla and Stenflo, 2005; Mikhailovskii *et al.*, 1989], but the understanding of ion cyclotron turbulence is not as developed despite its importance to the near-Earth environment [Meredith *et al.*, 2003; Summers and Thorne, 2003; Summers *et al.*, 1998; McClements *et al.*, 1994]. An effective way to investigate the properties of ion cyclotron turbulence in the near-Earth environment is to use it as a laboratory to seed the turbulence and closely monitor its evolution and signatures.

[3] In this article, we discuss the concept and feasibility of seeding ion cyclotron turbulence by neutral gas release in the magnetosphere perpendicular to the local magnetic field. Our analysis and estimates indicate that it is possible to induce intense ion cyclotron instability in a large volume in the near-Earth environment. The waves generated are the highly oblique ($k_{\perp} \gg k_z$, where k_{\perp} and k_z are the wave vectors across and

along the ambient magnetic field, respectively), short wavelength shear Alfvén waves amplified around harmonics of the ion cyclotron frequency of the injected species. The energy of these waves resides mostly in the sloshing motion of the ions, making them quasi-electrostatic in nature. An important nonlinear process is found to be the coalescence of two such short wavelength plasmons into a long wavelength plasmon with $k_{\perp} \sim k_z$. This nonlinear evolution converts the quasi-electrostatic waves into electromagnetic waves with interesting implications, especially for pitch angle scattering of trapped relativistic electrons. The coalescence process is the reverse of the decay of a long wavelength plasmon into two short wavelength plasmons recently discussed by Voitenko and Goossens [2005].

[4] The experiment we propose is based on release of an easily ionized vapor (such as lithium, cesium, etc.) from a satellite traversing the magnetospheric region of interest, such as the radiation belt. As we shall show, this procedure would result in the formation of a plasma cloud, and the plasma contained therein is far from thermodynamic equilibrium, with an anisotropic and population-inverted velocity distribution that is highly unstable to the spontaneous growth of large-amplitude waves. The free energy contained in this plasma is drawn directly and efficiently from the orbital kinetic energy which is greater by many orders of magnitude than the energy that could conceivably be supplied to waves by any electrically driven antenna in space [Inan *et al.*, 2003]. This concept grows out of the extensive experimental and theoretical studies, over several decades, of ionizable chemical releases in the magnetosphere [Brice, 1970; Bernhardt, 1992; Giles *et al.*, 1995] and more recent studies of electromagnetic turbulence in a multispecies plasma [Ganguli and Rudakov, 2004, 2005; Rudakov and Ganguli, 2005]. There has been interest since the 1970s in the use of chemical releases to enhance the

¹Plasma Physics Division, Naval Research Laboratory, Washington, District of Columbia, USA.

²Icarus Research Inc., Bethesda, Maryland, USA.

³National Research Council, Naval Research Laboratory, Washington, District of Columbia, USA.

⁴Department of Physics and Astronomy, University of Maryland, College Park, Maryland, USA.

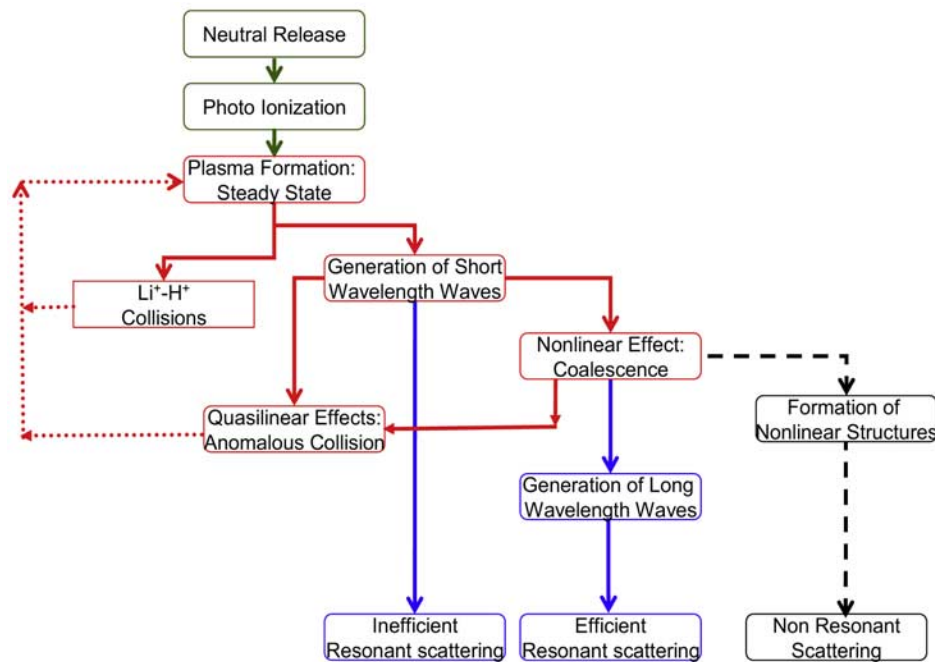


Figure 1. A schematic of the chain of key processes. The green and the blue color represent the input energy and the resulting signatures, respectively, whereas red represents the formation of the plasma steady state. The black dashed line represents a possibility currently under research.

growth of waves indigenous to the magnetosphere, such as the whistlers [Brice and Lucas, 1971; Cupperman and Landau, 1974; Ganguli et al., 1984]. However, the present scheme is fundamentally different in that it envisions designing the local ion distribution through shaped release of neutral gas and drawing on the free energy of the artificially created plasma cloud to grow the necessary waves. In the following, we first discuss the proposed method of seeding the waves around lithium ion cyclotron frequency harmonics in the magnetosphere and then discuss its linear and nonlinear evolution and observable signatures such as enhanced precipitation of relativistic electrons. Some of the details are reserved for the appendices. Figure 1 provides a schematic overview of the essential processes involved.

2. Neutral Gas Release Induced Turbulence at Low Altitudes

[5] Our objective is to seed electromagnetic lithium cyclotron turbulence with properties suitable for nonlinear phenomena, such as wave-wave coupling, pitch angle scattering, etc., in the low-altitude region where the ambient plasma β ($= 8\pi n\kappa T/B^2$) is low. This may be achieved by creating a plasma with a ring distribution of perpendicular velocities [McClements et al., 1994] and/or an anisotropic distribution with $v_{\perp} > v_z$ for most ions. Now we show how this can result from the release of an ionizable gas and examine the stability in such a plasma.

2.1. Creation of Plasma With a Ring Ion Velocity Distribution

[6] We first consider how the release of neutral gas from a satellite leads naturally to the formation of plasma with a ring and anisotropic ion distribution. Such distributions are

in fact known to be created by shuttle exhaust in the ionosphere [Bernhardt and Sulzer, 2004; Bernhardt et al., 1998] and also in the comet tails [Hizanidis et al., 1988; Shapiro et al., 1993]. Several release scenarios are possible. We consider vaporized lithium release from nozzles on a satellite body directed perpendicular to the trajectory of the satellite in equatorial orbit at the desired altitude as shown schematically in Figures 2a and 2b. The lithium gas jets are continuously injected from K nozzles over a release period τ_R and with a release speed V_R with respect to the satellite.

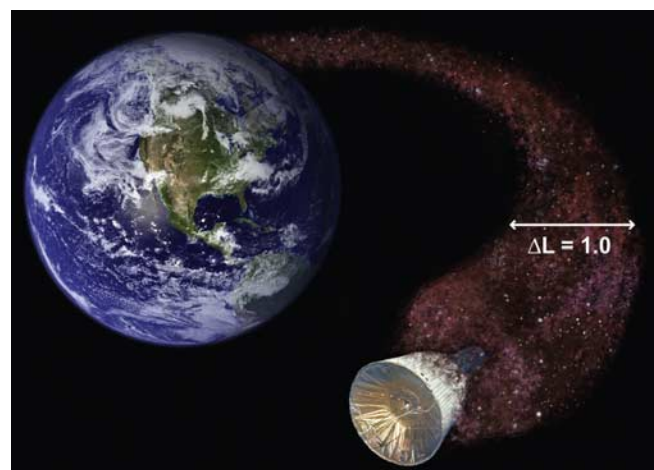


Figure 2a. A schematic of the neutral lithium gas injection. The gas is released radially normal to the satellite trajectory in the Earth's equatorial plane where the ambient magnetic field is perpendicular to the satellite trajectory. With a release speed of $V_R \sim 1$ km/s, it is possible to create a lithium cloud of width $\Delta L \approx 1$ (i.e., 6000 km) which can be photoionized into a plasma cloud.

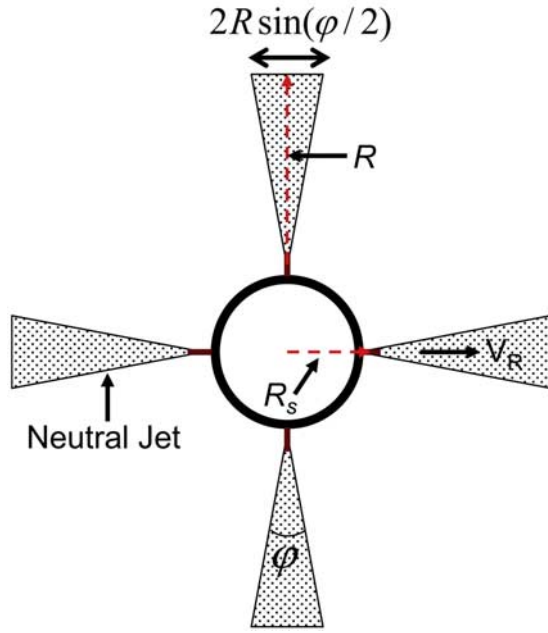


Figure 2b. A schematic of the cross section perpendicular to the satellite motion. R_s is the satellite dimension. Shown here are four nozzles injecting conical jets of neutral lithium with velocity V_R perpendicular to the satellite motion. The nozzles operate simultaneously and continuously until all neutrals are released. The number of nozzles (K) may be altered if needed.

The satellite orbital speed is V_s . Thus a cloud of neutral lithium will be formed whose center of mass will follow the satellite around its orbit. The dimension of the conical neutral cloud from each jet at time t will be $R = V_R t$ along the jet and $2R \sin(\phi/2)$ in diameter, where ϕ is the total angular spread of the jet in vacuum and is assumed to be small (see Figure 2b). The atoms in the neutral cloud are photoionized over the characteristic ionization time T_i . For $t \geq T_i$, a quasi steady state will be established in which the conical neutral cloud structures of size $R_{\max} = V_R T_i$ formed by K nozzles move with the satellite velocity. If N_n neutral atoms are released continuously over a period τ_R by all the nozzles, then the rate per nozzle is $N_n/K\tau_R$. The quasi-stationary neutral cloud density n_n at a given radial distance from the satellite $R \gg R_s$, where R_s is the satellite dimension, can be found by equating the neutral flux from a nozzle, $n_n V_R \pi R^2 \sin^2(\phi/2)$, to $N_n/K\tau_R$. For large R , the neutral density falls off rapidly as $\exp(-R/R_{\max})$ because of ionization. Thus the density of the neutrals at any position $R \gg R_s$ can be estimated to be $n_n = N_n \exp(-R/R_{\max}) / K V_R \tau_R \pi R^2 \sin^2(\phi/2)$.

[7] As the neutral cloud follows the satellite trajectory, the atoms are ionized and become attached to a magnetic field line. Consequently, they can no longer move across the field lines. They form a plasma with ring distribution in velocity space which is unstable to electromagnetic waves as discussed in section 2.3. At any given point, the plasma is formed over the average duration of $\tau_p = R \sin(\phi/2) / V_s$ when the neutral cloud is resident at this point. The lithium ions are slowed down because of the lithium-hydrogen collision with frequency ν_{Li-H} thereby leading to thermal dissipation of the

energy. This can reduce the free energy available to sustain the waves. In addition to the Coulomb collisions, the wave-generated anomalous collision can also have a stabilizing effect on the waves. Including these collision effects, the instantaneous lithium ion density n_{Li} which supports the instability is determined by

$$\frac{dn_{Li}}{dt} = \frac{n_n}{T_i} - \nu_{Li-H} n_{Li} - \nu_a n_{Li}, \quad (1a)$$

where ν_a is the anomalous collision frequency associated with the wave-particle interactions. Solving equation (1a) with the neutral density in jets described above, the lithium ion density actively supporting the instability at the end of the plasma formation time at $t = \tau_p$ is found to be

$$n_{Li} = \frac{N_n}{K V_R \tau_R \pi R^2 \sin^2(\phi/2)} \frac{\exp(-R/R_{\max})}{\nu T_i} (1 - \exp(-\nu \tau_p)). \quad (1b)$$

Here $\nu \equiv \nu_a + \nu_{Li-H}$. From equation (1b), it can be shown that the maximum number of active lithium ions available to support the turbulence are located at the radius R_1 such that $\nu \tau_p(R_1) \sim 1$. Thus most of the energy will be released at R_1 .

[8] The deposited plasma thus occupies a swath along the trajectory of the satellite, gradually falling off in density as the neutral gas source is depleted. This plasma will have no mean flow velocity. However, all the lithium ions are created with a large velocity in the equatorial plane. After spinning up around the magnetic field B , this leads to a narrow distribution of ion velocities perpendicular to B , centered just below V_s . We approximate the lithium ion distribution function by

$$f_0 = \frac{1}{(2\pi)^{3/2} v_{\perp}^2 v_z} \exp\left(-\frac{(v_{\perp} - V_s)^2}{2v_{\perp}^2} - \frac{v_z^2}{2v_z^2}\right). \quad (2)$$

The perpendicular energy $E_{\perp} = m_{Li} V_s^2 / 2$, which is equal to the injection energy, and $v_{\perp}, v_z \ll V_s$ initially. For lithium ions (Li^7) released at the satellite speed $V_s = 7$ km/s, the injection energy per ion is equal to 2.8×10^{-12} ergs, which corresponds to $E_{\perp} \sim 1.75$ eV.

[9] The distribution function of the newly formed ions is both highly anisotropic and annular in the transverse velocity. Both of these features are known to drive plasma instabilities. The anisotropy factor $\theta \equiv E_{\perp} / T_z$, where T_z is the temperature along the magnetic field, vastly exceeds typical values of order 1.5–3 in the ambient radiation belts [Kennel and Petschek, 1966]. This annular distribution leads to particularly robust instabilities, since the entire ion distribution drives the unstable wave, rather than only a small selection of ions whose velocity is in resonance with the wave. As we shall show in section 2.3, this distribution leads to instability of the highly oblique shear Alfvén waves near the lithium cyclotron harmonics.

2.2. Estimate of Lithium Ion Density

[10] To be more specific, we target the volume of space between $L = 1.5$ – 2.5 as the region of interest in which to localize the turbulence and use the conditions at $L = 2$ for making estimates. The ambient magnetic field here is $B = 0.04$ G, ion (mainly hydrogen along with a small quantity of helium) and electron temperatures are roughly 0.3 eV during night and 0.5 eV during day, hydrogen density

$n_H = 3 \times 10^3/\text{cc}$, and $\beta = 4 \times 10^{-5}$. Consider the release of 1 ton of lithium which corresponds to 10^{29} neutral lithium atoms. Since we want most of the energy introduced by the release to be channeled into the waves and turbulence, we must minimize the loss of energy due to thermalization by lithium-hydrogen collision. This may be achieved by ensuring that the plasma formation time at a given point does not exceed the thermalization time, $1/\nu_{\text{Li-H}} \approx 165$ s. We shall see in section 3 that nonlinear wave-wave coupling is a prominent feature of the evolution that competes with wave-particle interactions. Hence the time-scale (ν_a^{-1}) associated with wave-particle interaction is not the linear growth time (γ^{-1}) as in a quasi-linear model but much longer making $\gamma > \nu_a$. This, along with our choice of $\tau_p \leq 1/\nu_{\text{Li-H}}$, leads to the hierarchy $\gamma > \nu_a > \nu_{\text{Li-H}}$. Although $\nu_a = g\nu_{\text{Li-H}}$ with $g > 1$, the exact value of g can only be determined by numerical simulation which is beyond the scope of this article. To estimate n_{Li} , we assume that the wave-particle interaction is twice as fast as the thermalization, i.e., $g = 2$ so that $\nu = 3\nu_{\text{Li-H}} \sim 1/55 \text{ s}^{-1}$, but a different value of g can be accommodated by adjusting the number of nozzles K , $\sin(\phi/2)$, τ_R , etc., to ensure the desired magnitude of n_{Li} . To estimate the average lithium density at $R_{\text{max}}/2$, we choose $K = 4$, $V_R = 1 \text{ km/s}$, $\sin(\phi/2) \sim 0.25$, $\tau_R = 5 \times 10^3 \text{ s}$, and $\tau_p = (R_{\text{max}}/2)\sin(\phi/2)/V_s$. For $\nu\tau_p = 1$, equation (1b) yields the lithium ion density in jets which is active in supporting the waves to be $n_{\text{Li}} \sim 100/\text{cc}$. Since the background hydrogen density at $L = 2$ is $n_H \sim 3000/\text{cc}$, the ratio $n_{\text{Li}}/n_H \sim 0.03$. Note that the total lithium density, which includes the ring distribution and the thermalized components, i.e., $n_{\text{Li}}^{\text{Total}} = n_n\tau_p/T_i$, is larger.

[11] When ionized, the 10^{29} atoms of ejected lithium with 1.75-eV energy each introduces a net energy of approximately 30 GJ into the medium which corresponds to an average power of 10 MW over the lithium ionization time of 3000 s. This is an enormous source of energy, and it is to be emphasized that this energy derives directly and efficiently from the orbital kinetic energy, not from any electrical or chemical energy source carried on the vehicle. If even a fraction of this energy is converted into electromagnetic turbulence, it would lead to large amplitude electromagnetic waves with easily observable signatures. In the following section, we examine and quantify the characteristics of the turbulence and its consequences.

2.3. Electromagnetic Ion Cyclotron Instability

2.3.1. Linear Properties

[12] In Appendix A, we give the details of the derivation of the dispersion relation for highly oblique shear Alfvén waves near the lithium ion cyclotron frequency. These are linearly polarized waves which results from the coupling of left and right circularly polarized modes for $k_{\perp} \gg k_z$. The simplified version [equation (A21)] of this dispersion relation can be written as

$$D(\omega, k) = \frac{k_z^2 V_A^2}{\omega^2} \left(1 + \frac{k_x^2 c^2}{\omega_{pe}^2} \frac{1}{\zeta^2 Z'(\zeta)} \right)^{-1} - \sum_{\alpha, l} \frac{n_{\alpha} m_{\alpha}}{n_H m_H} \frac{l^2 \Omega_{\alpha}^2}{l^2 \Omega_{\alpha}^2 - \omega^2} \frac{2\Gamma_l(b_{\alpha})}{b_{\alpha}} + \sum_l \frac{n_{\text{Li}} m_{\text{Li}}}{n_H m_H} \frac{dJ_l^2(\sigma_s)}{\sigma_s d\sigma_s} \frac{l^2 \Omega_{\text{Li}}^2}{\omega(\omega - l\Omega_{\text{Li}})} = 0, \quad (3)$$

where the subscripts α , e, and Li indicate ambient ion species (hydrogen and helium), electron, and lithium, respectively. Helium density is about 5% of hydrogen at $L = 2$ [Craven *et al.*, 1997]. Since the instability lifetime is designed to be less than the thermalization time by restricting $\tau_p \leq 1/\nu_{\text{Li-H}}$, we ignore the thermalized lithium component from the dispersion relation by setting $n_{\text{Li}} = 0$ in equation (A21). $Z(\zeta)$ is the plasma dispersion function, $Z' = dZ(\zeta)/d\zeta$, $\zeta = \omega/\sqrt{2}k_z v_{te}$, $v_{t\alpha} = \sqrt{T_{\alpha}/m_{\alpha}}$, $b_{\alpha} = (k_x \rho_{\alpha})^2/2$, $\rho_{\alpha} = v_{t\alpha}/\Omega_{\alpha}$, $\Gamma_l(b) = I_l(b)\exp(-b)$, where $I_l(b)$ are the modified Bessel function, $\sigma_s = k_{\perp} V_s/\Omega_{\text{Li}}$, and J_l are the Bessel functions. It can be shown that the energy density of these waves becomes negative because $\partial\omega D(\omega)/\partial\omega|_{\omega=\omega_r} < 0$ when $dJ_l^2(\sigma_s)/d\sigma_s$ is negative which is a necessary condition for wave growth. Since $dJ_l^2(\sigma_s)/d\sigma_s < 0$ for $\sigma_s > 1$, this instability occurs for short perpendicular wavelengths with $k_{\perp} \gg k_z$. This differentiates these waves from the classical electromagnetic ion cyclotron (EMIC) waves for which typically $k_{\perp} \ll k_z$. To determine the wave frequency, we ignore the helium and lithium species because their mass densities are much smaller than that of the hydrogen to obtain

$$\omega^2 = \frac{k_z^2 V_A^2}{\frac{2\Gamma_1(b_H)}{b_H} \left(1 + \frac{k_x^2 c^2}{\omega_{pe}^2} \frac{1}{\zeta^2 Z'(\zeta)} \right) + \frac{k_x^2 c^2}{\omega_{pH}^2}}. \quad (4)$$

In the typical MHD limit, i.e., long wavelength and cold plasma corresponding to $(2\Gamma_1/b_H) = 1$ and $\zeta^2 Z'(\zeta) = 1$, equation (4) reduces to the expression for the inertial shear Alfvén waves,

$$\omega_r = k_z V_A \left(1 - \frac{k_x^2 c^2}{2\omega_{pe}^2} \right), \quad (5)$$

but for short wavelengths and a cold plasma, the real frequency is

$$\omega_r^2 = \frac{k_z^2 V_A^2}{\left(1 + \frac{k_x^2 c^2}{\omega_{pe}^2} + \frac{k_x^2 c^2}{\omega_{pH}^2} \right)}. \quad (6)$$

[13] To obtain the growth rate γ , analytically, we impose the double resonance condition that the real frequency ω_r is determined by both equation (4) and the condition $\omega_r = l\Omega_{\text{Li}}$. Under this condition, the growth rate is given by

$$\frac{\gamma}{l\Omega_{\text{Li}}} = \frac{1}{2} \left[-\Delta + \sqrt{\Delta^2 + \frac{n_{\text{Li}} m_{\text{Li}}}{n_H m_H} \left| \frac{dJ_l^2(\sigma_s)}{\sigma_s d\sigma_s} \right| \frac{b_H}{\Gamma_1(b_H)} \left(\frac{\Omega_H^2 - l^2 \Omega_{\text{Li}}^2}{\Omega_H^2} \right)^2} \right], \quad (7)$$

where $l < m_{\text{Li}}/m_H$ and electron Landau damping effect is included through

$$\Delta = \zeta^3 \exp(-\zeta^2) \left(\frac{\Omega_H^2 - l^2 \Omega_{\text{Li}}^2}{2\Omega_H^2} \right). \quad (8)$$

[14] Since these waves have negative energy density, Landau damping does not suppress them but can lower

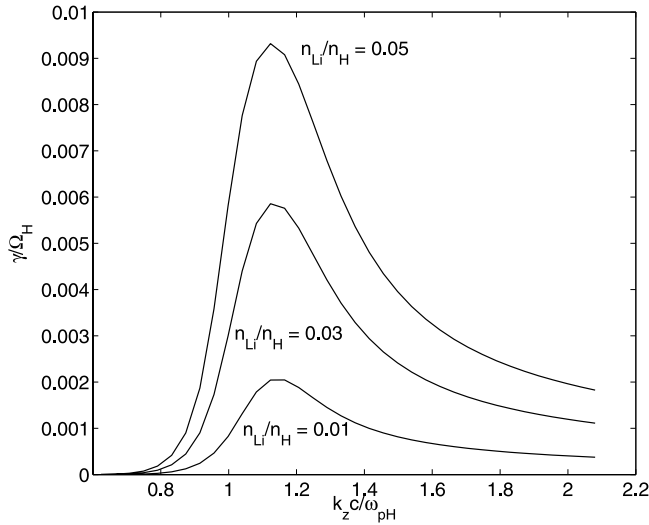


Figure 3. Growth rate, obtained by solving equation (3), versus parallel wave vector for different density ratios ($n_{\text{Li}}/n_{\text{H}}$) for the parameters relevant to $L = 2$. The frequency is chosen to be around the third lithium harmonic ($l = 3$).

the growth rate. Equation (7) indicates that there is no threshold for the instability as long as $\tau_p \leq 1/\nu_{\text{Li-H}}$ because the thermalized lithium ions which can damp the waves are negligible. Plots of $dJ_1^2(\sigma_s)/d\sigma_s$ against σ_s indicate that the negative peak of $dJ_1^2(\sigma_s)/d\sigma_s$ occurs roughly for $\sigma_s^* = k_x^* V_s / \Omega_{\text{Li}} \approx (l + 2)$. As mentioned earlier, the parameters of interest at $L = 2$ are $n_0 \sim 3 \times 10^3$ cc, $T_{\text{H}} = T_e \sim (0.3-0.5)$ eV (night-day), $B_0 \sim 0.04$ G, $V_A \sim 1.6 \times 10^3$ km/s, $V_s = 7$ km/s, and $\beta \sim 4 \times 10^{-5}$. Also, $m_{\text{Li}} = 7m_{\text{H}}$ and $m_{\text{Li}} V_s^2 / 2 \sim 1.75$ eV. These imply that

$$b_{\text{H}}^* = \frac{k_x^* v_{\text{H}}^2}{2\Omega_{\text{H}}^2} \approx (l + 2)^2 \frac{m_{\text{H}}}{m_{\text{Li}}} \frac{T_{\text{H}}}{m_{\text{Li}} V_s^2} \ll 1, \quad (9)$$

for lower harmonics, but

$$\frac{k_x^2 c^2}{\omega_{\text{pe}}^2} \approx (l + 2)^2 \frac{m_e m_{\text{H}}}{m_{\text{Li}}^2} \frac{V_A^2}{V_s^2} \gg 1. \quad (10)$$

It follows that $\zeta \sim 1/b_{\text{H}}^* > 1$, which implies that Landau damping is weak especially for the lower harmonics. Equation (7) indicates that for weak Landau damping (i.e., $\Delta \rightarrow 0$), the instability growth rate varies as the square root of the lithium-to-hydrogen-density ratio, while for the strong Landau damping case, it varies linearly with the density ratio.

[15] Figure 3 is a plot of growth rate versus parallel wave vector for different density ratios ($n_{\text{Li}}/n_{\text{H}}$) for the parameters relevant to $L = 2$. The frequency is chosen to be around the third lithium harmonic ($l = 3$). The value of $k_x c / \omega_{\text{pH}} = 170$. It was obtained by numerical solution of equation (3) including helium with $n_{\text{He}}/n_{\text{H}} = 0.05$. Figure 3 shows that the growth occurs for short perpendicular wavelengths but large parallel wavelengths.

[16] Figure 4 is a plot similar to Figure 3 where we use $n_{\text{Li}}/n_{\text{H}} = 0.03$ and plot the growth rates near different

lithium cyclotron harmonics. For $l = 1, 2, 3, 4$, and 5 , the corresponding values of $k_x c / \omega_{\text{pH}} = 85, 135, 170, 210$, and 245 , respectively. We find that as the harmonic number increases, the range of unstable k_z also increases, but the typical value of the ratio k_z/k_x where the instability peaks remains around $0.01-0.03$. This can be understood from the dispersion relation equation (6). For Li^7 $\omega_r = l\Omega_{\text{Li}} \cong \Omega_{\text{H}}/7$, equation (6) reduces to $(1 - (l/7)^2)\bar{k}_z^2 = 1 + \bar{k}_x^2 m/m_{\text{H}}$, where $\bar{k}_{z,x} \equiv k_{z,x} c / \omega_{\text{pH}}$. Neglecting “1” in the right-hand side, we get $(k_x/k_z) \cong \sqrt{(m_{\text{H}}/m_e)(1 - (l/7)^2)}$.

2.3.2. Trapping of Waves in Magnetospheric Cavity

[17] It can be shown that these waves, generated around the equator where the Earth’s magnetic field is weakest, are reflected as they propagate along the magnetic field in each hemisphere. Since their perpendicular group velocity, obtained from equation (6) for $k_z^2 c^2 \sim \omega_{\text{pH}}^2$ and $k_x^2 c^2 > \omega_{\text{pe}}^2$, $\partial\omega/\partial k_x = V_A(k_z/k_x) \sim V_A/100$, is small, the radial transport of these waves is not large. Consequently, the waves are trapped along the magnetic field and will oscillate between the two turning points. The formation of such oscillator will effectively increase the turbulence lifetime, which, as shown in section 5, will increase the efficiency of pitch angle scattering. It is known that in a multi-ion species plasma, such as hydrogen and helium, reflection of waves below the ion cyclotron frequency occurs when the Buchsbaum frequency, $\omega_{\text{B}}^2 = \Omega_{\text{H}}\Omega_{\text{He}}(n_{\text{H}}m_{\text{H}} + n_{\text{He}}m_{\text{He}})/(n_{\text{H}}m_{\text{He}} + n_{\text{He}}m_{\text{H}})$, equals to the wave frequency as the wave propagates along the field lines [Rauch and Roux, 1982; Roux et al., 1984]. In this case, each harmonic of the lithium gyrofrequency Ω_{Li} that is above the Buchsbaum frequency ω_{B} reflects at some point along the field line. Consequently, the waves are trapped between two symmetric turning points forming an oscillator and are amplified during transits through the region of instability. Lower harmonics which are not trapped will be eventually lost. A more detailed analysis

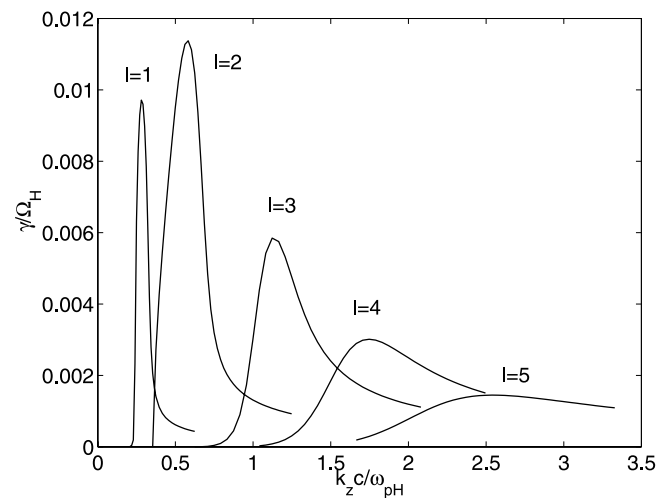


Figure 4. Growth rate, obtained by solving equation (3), for harmonics of the lithium gyrofrequency ($l = 1-5$) versus parallel wavelength. The density ratio is held fixed at $n_{\text{Li}}/n_{\text{H}} = 0.03$. The spread in widths near the maximum growth rate indicates that Landau damping is weaker for lower harmonics than for higher harmonics.

of this topic including Landau and collisional dampings, behavior of the wave equation near the Buchsbaum frequency, the quality of reflection, etc., during propagation outside the region of creation will be published in a subsequent article.

2.3.3. Energy Partition

[18] The energy of these waves, W , is largely in the kinetic energy of the particles, i.e., hydrogen and electrons. This can be seen by comparing the particle kinetic energy and the field energy (see Appendix A),

$$\frac{(m_e n_e |v_{1z}|^2 + m_H n_H |v_{1y}|^2) / 2}{|B_{1y}|^2 / 8\pi} = \left(1 + \frac{2k_x^2 c^2}{\omega_{pe}^2}\right) \gg 1. \quad (11)$$

Although the magnetic fluctuations of these waves are small, they are electromagnetic in nature. This is unlike the classical MHD Alfvén waves with $k_x \rightarrow 0$ in which the energy in the particles is equal to that in the fluctuating fields.

2.3.4. Compressibility

[19] A similar departure from classical behavior is also found in the compressibility of the oblique shear Alfvén waves near the ion cyclotron frequency. To see this, we note that the velocity fluctuations associated with the shear Alfvén waves are given by

$$v_{yi} = \frac{cE_{x1}}{B_0} \left(1 - \frac{\omega^2}{\Omega_H^2}\right)^{-1}, \quad (12a)$$

$$v_{xi} = -i \frac{\omega}{\Omega_H} \frac{cE_{x1}}{B_0} \left(1 - \frac{\omega^2}{\Omega_H^2}\right)^{-1}, \quad (12b)$$

$$v_{ye} = \frac{cE_{x1}}{B_0}, \quad (12c)$$

$$v_{ze} = -i \frac{e}{m} \frac{E_{z1}}{\omega}. \quad (12d)$$

From the ion continuity equation, we get the density perturbation

$$\frac{n_1}{n_0} = \frac{k_x v_{xi}}{\omega} = -i \frac{k_x}{\Omega_H} \frac{cE_{x1}}{B_0} \left(1 - \frac{\omega^2}{\Omega_H^2}\right)^{-1} = -i \frac{k_x v_{yi}}{\Omega_H} = -i \frac{k_x c}{\omega_{pH}} \frac{v_{yi}}{V_A}. \quad (13)$$

Thus while the classical Alfvén waves for which $k_x \rightarrow 0$ is incompressible, the oblique shear Alfvén waves of our interest is compressible.

2.3.5. Onset of Nonlinear Effects

[20] Finally, we note that the shear Alfvén waves are generated with large amplitude, and hence the nonlinear effects become important. Assuming about 1% of the energy released goes into the waves, we see that $W \sim 0.01 m_{Li} n_{Li} V_s^2 \sim 10^{-7} B_0^2 / 8\pi$ for $L = 2$ conditions. The corresponding number for the natural background during solar storms is $10^{-13} B_0^2 / 8\pi$. Thus the wave amplitudes generated by the neutral gas release will be 3 orders of

magnitude larger than the normal background fluctuations in the radiation belt. Therefore a careful analysis of the nonlinear evolution becomes necessary.

3. Nonlinear Evolution of the Induced Shear Alfvén Waves

[21] As discussed in section 2.2, the neutral injection process introduces energy (approximately 30 GJ for 1 ton of lithium) into the medium which can be accessed to pump and sustain turbulence, whereas in section 2.3, we studied the onset condition and linear properties of the shear Alfvén waves. We found that these waves are generated with short perpendicular wavelength but large amplitudes, which make them weakly electromagnetic but likely nonlinear. The key nonlinear issues of interest to us are as follows: Can the nonlinear process lead to the generation of long wavelength electromagnetic wave, and how do these waves affect the plasma environment? What are the controlling parameters? In the absence of dissipation mechanisms, such as collisions, Landau damping, etc., turbulence, maintained over a sufficiently long period of time, can distribute energy into all available wave vectors of the shear Alfvén waves as well as other possible normal modes, such as the whistler, magneto-sonic, etc., through nonlinear processes. Several nonlinear processes may be operative. Estimates of their rates indicate that in a low β plasma, such as the one we consider, coalescence of short wavelength modes into long wavelength modes that are unaffected by electron Landau damping is the dominant process. In the following, we consider this process in somewhat more detail but defer a comprehensive nonlinear study to a future article.

[22] In the nonlinear wave-wave interaction, the plasmon energy and momentum conservation law, i.e., $\omega_1(k_1) \pm \omega_2(k_2) = \omega_3(k_3)$ and $\vec{k}_1 \pm \vec{k}_2 = \vec{k}_3$, must be satisfied. We showed in the previous section that the shear Alfvén waves in a cold hydrogen plasma are described by the dispersion relation

$$D \equiv \frac{\omega_{pH}^2}{\Omega_H^2 - \omega^2} \left(1 + \frac{k_\perp^2 c^2}{\omega_{pe}^2}\right) - \frac{k_z^2 c^2}{\omega^2} = 0. \quad (14)$$

We replace k_x by k_\perp because, in general, turbulence proceeds in three dimensions. Equation (14) can be solved to obtain

$$\omega^2 = k_z^2 V_A^2 \left/ \left(1 + \frac{k_\perp^2 c^2}{\omega_{pe}^2} + \frac{k_z^2 c^2}{\omega_{pH}^2}\right)\right. \quad (15)$$

Defining $\omega/\Omega_H \rightarrow \bar{\omega}$, $k_{z,\perp} c/\omega_{pH} \rightarrow \bar{k}_{z,\perp}$ in equation (15), we obtain

$$\bar{\omega} = |\bar{k}_z| / \left(1 + \bar{k}_\perp^2 m_e/m_H + \bar{k}_z^2\right)^{1/2}. \quad (16)$$

The plasmon “energy,” i.e., the frequency ω , is positive, whereas the projections of the “momentum,” i.e., the wave vector \vec{k} , can be positive or negative. Since the waves generated by the lithium release have short wavelengths $\bar{k}_\perp^2 \gg m_H/m_e$, $\bar{k}_z^2 > 1$, we can simplify equation (16) to

$$\bar{\omega} = |\bar{k}_z| / \left(\bar{k}_\perp^2 m_e/m_H + \bar{k}_z^2\right)^{1/2}. \quad (17)$$

[23] Let two such degenerate shear Alfvén waves, denoted by subscripts 1 and 2, coalesce to generate another shear Alfvén wave, denoted by subscript 3, such that $\vec{k}_{\perp 3} = \vec{k}_{\perp 1} + \vec{k}_{\perp 2} \ll \vec{k}_{\perp 1}$ and $k_{z3} = k_{z1} \pm k_{z2}$. Then the plasmon energy-momentum conservation law for the three interacting waves is given by,

$$\frac{|\vec{k}_{z1}|}{(\bar{k}_{\perp 1}^2 m_e/m_H + \bar{k}_{z1}^2)^{1/2}} + \frac{|\vec{k}_{z2}|}{(\bar{k}_{\perp 2}^2 m_e/m_H + \bar{k}_{z2}^2)^{1/2}} = \frac{|\vec{k}_{z3}|}{(1 + \bar{k}_{\perp 3}^2 m_e/m_H + \bar{k}_{z3}^2)^{1/2}}, \quad (18)$$

We consider the special case, $\bar{k}_{z3} = \bar{k}_{z1} - \bar{k}_{z2} < \bar{k}_{z1}$, $\bar{k}_{\perp 3} = \bar{k}_{\perp 1} - \bar{k}_{\perp 2} \ll \bar{k}_{\perp 1}$, $\bar{k}_{\perp 1} \gg m_H/m_e$ but $\bar{k}_{\perp 3} \ll m_H/m_e$. Hence the solution of equation (18) is

$$\frac{|\vec{k}_{z1} - \bar{k}_{z2}|}{|\vec{k}_{z1}| + |\vec{k}_{z2}|} = \frac{|\vec{k}_{z1} - \bar{k}_{z2}|}{2|\vec{k}_{z1}|} = \frac{(1 + \bar{k}_{z3}^2)^{1/2}}{(\bar{k}_{\perp 1}^2 m_e/m_H + \bar{k}_{z1}^2)^{1/2}} \approx \frac{1}{(\bar{k}_{\perp 1}^2 m_e/m_H)^{1/2}}. \quad (19)$$

The last equality results because $\bar{\omega}_1 \sim \bar{\omega}_2 \sim \bar{\omega}_3 \sim \bar{k}_{z3} \sim O(1)$ and $(\bar{k}_{\perp 1}^2 m_e/m_H)^{1/2} > \bar{k}_{z1} > 1$. From equations (18) and (19), we find that $\omega_1 = \omega_2 = \omega_3/2$ and $\omega_1 - \omega_2 \approx \omega_3/(\bar{k}_{\perp 1}^2 m_e/m_H)^{1/2}$. Thus we see that the highly oblique shear Alfvén waves can decay into the usual shear Alfvén waves with $\bar{k}_{\perp 3} \ll (m_H/m_e)^{1/2}$. While we found the mother waves to be weakly electromagnetic in nature with most of the wave energy concentrated in the particles [see section 2.3, equation (11)], the long wavelength daughter waves are electromagnetic with wave energy equally partitioned between the particles and the fluctuating magnetic fields. This has an important consequence as far as pitch angle scattering is concerned as discussed in section 5.

[24] The turbulence can also lead to the generation of the magnetosonic waves. We demonstrate this for a particular case using the dispersion relation for the magnetosonic wave with $k_{z3} = 0$, which has no resonance at the hydrogen cyclotron frequency. In normalized values, it is

$$\bar{\omega}_3 = \bar{k}_{\perp 3}. \quad (20)$$

Let $\vec{k}_{\perp 1} + \vec{k}_{\perp 2} = \vec{k}_{\perp 3} \ll \vec{k}_{\perp 1}$, $k_{z1} + k_{z2} = k_{z3} = 0$. Then the plasmon energy-momentum conservation law for two shear Alfvén waves coalescing to generate a magnetosonic wave, i.e., $\omega_3 = \omega_1 + \omega_2$, is

$$\frac{|\vec{k}_{z1}|}{(\bar{k}_{\perp 1}^2 m_e/m_H + \bar{k}_{z1}^2)^{1/2}} + \frac{|\vec{k}_{z2}|}{(\bar{k}_{\perp 2}^2 m_e/m_H + \bar{k}_{z2}^2)^{1/2}} = \bar{k}_{\perp 3}. \quad (21)$$

Equation (21) gives

$$\bar{k}_{\perp 3} = \frac{2|\vec{k}_{z1}|}{(\bar{k}_{\perp 1}^2 m_e/m_H + \bar{k}_{z1}^2)^{1/2}}. \quad (22)$$

Since for the mother waves $\omega_1 \approx \omega_2 < \Omega_H$, the frequency of the daughter waves, represented by equation (20), is

approximately $\omega_3 < 2\Omega_H$. Therefore it follows that $\bar{k}_{\perp 3}$ is on the order of unity. Thus both $\bar{k}_{\perp 3}$ and \bar{k}_{z3} are restricted. This implies that the volume these daughter waves occupy in k space is limited. Hence the energy pumped into the daughter magnetosonic waves is smaller than in the daughter Alfvén waves.

3.1. Coalescence of Shear Alfvén Waves

[25] We now consider the rate of coalescence of the shear Alfvén waves. The nonlinear interaction of the mother waves leads to the generation of a second-order current as explained in Appendix B. The rate of coalescence is determined by calculating the power due to the second-order current and electric field when the daughter wave is in resonance with the mother waves (i.e., $\omega_3 = \omega_1 + \omega_2$ and $\vec{k}_3 = \vec{k}_1 + \vec{k}_2$). When the second-order current is included, the general equation for the shear Alfvén waves is given by

$$k_z^2 E_x - k_x k_z E_z - \frac{4\pi}{c^2} i\omega \sigma_{xx} E_x = k_z^2 E_x - \frac{4\pi}{c^2} i\omega \sigma_{xx} E_x \left(1 - \frac{k_x^2 c^2}{4\pi i\omega \sigma_{zz}}\right) = \frac{4\pi}{c^2} i\omega j_x^{(2)}, \quad (23)$$

where $j_x = \sigma_{xx} E_x$, $j_z = \sigma_{zz} E_z$, and σ_{xx} and σ_{zz} are the components of the plasma conductivity tensor. If $j_x^{(2)} = 0$, then equation (23) reduces to equation (A7). For simplifying the analysis we will consider the special case where $|k_{\perp 3}| = |k_{\perp 1}| - |k_{\perp 2}| \ll |k_{\perp 1}|$, $\bar{k}_{\perp 3} \ll m_H/m_e$. In addition, wherever possible, we neglect terms proportional to $\bar{k}_{\perp 3}$ and assume that $\vec{k}_{\perp 1} = -\vec{k}_{\perp 2}$; that is, the wave vectors of the mother waves are nearly in the same plane, say the (x, z) plane. We calculate the rate of the coalescence of two mother waves with $k_{x1} \approx -k_{x2}$ which generates a daughter wave with $k_{x3} \ll k_{x1}$ but $k_{z3} \gg k_{z1}$. Under these conditions, the daughter waves are described by the simplified form of equation (23),

$$k_{z3}^2 E_x - \frac{4\pi}{c^2} i\omega_3 \sigma_{xx} E_x = \frac{4\pi}{c^2} i\omega j_x^{(2)}. \quad (24)$$

[26] We obtain $j_x^{(2)}$ by solving the momentum balance equation [equation (B1)] for the plasma and $E^{(2)}$ by solving equation (24). Using these quantities, the rate of coalescence, i.e., $j_x^{(2)} E^{(2)}$, can be calculated. The detailed analysis is given in Appendix B. The rate of coalescence for two short wavelength mother waves into a long wavelength daughter wave (or equivalently, the rate of generation of the daughter waves) is found to be [equation (B18)],

$$\left(\frac{dW_3}{d(\Omega_H t)}\right)_{2D} \sim \frac{\omega_3^5}{\Omega_H^5} \frac{m_H}{m_e} \frac{W_1^2}{B_0^2/8\pi}. \quad (25)$$

In deriving equation (25), we have assumed a uniform plasma and thus ignored the nonlocal effects which will be addressed in a subsequent article. Here W_1 and W_3 are the energy densities of the mother and daughter waves. The subscript ‘‘2D’’ indicates that for this interaction, the mother and daughter wave vectors are all in one plane. Note that this process is ignorable for the low-frequency ($\omega \ll \Omega_H$) Alfvén waves, i.e., in the MHD limit.

[27] In contrast to the above, the coalescence of the mother waves can give rise to the long wavelength magnetosonic waves

in the usual MHD limit with $k_{\perp 3}, k_{z3} \sim \omega_{pH}/c$. In this process, the daughter waves are not in the same plane as the mother waves, and the interaction takes place in three dimensions. The rate for this process is estimated in equation (B21). Taking the ratio of equation (B21) to equation (25), we find

$$(dW_3/dt)_{3D}/(dW_3/dt)_{2D} \approx (m_e/m_H)(\Omega_H/\omega_3)^4 \ll 1, \quad (26)$$

which indicates that for our case where $\omega_3/\Omega_H \sim 1$, the decay into daughter shear Alfvén waves will dominate over the decay into magnetosonic waves.

[28] In the traditional treatment of the low-frequency ($\omega/\Omega_H \ll 1$) Alfvénic turbulence, the energy flows from long to short scales by the cascade of energy transport. At each step, the wave scale size is approximately halved and the frequency doubled [Onishchenko *et al.*, 2003; Mikhailovskii *et al.*, 1989]. In contrast, in our higher frequency ($\omega/\Omega_H \sim 1$) case, the wave energy is distributed in only a few steps over all wavelengths, in particular, daughter waves are generated with long wavelength, i.e., $\bar{k}_{\perp}(m_e/m_H)^{1/2} \ll \bar{k}_z$.

[29] For the nonlinear process to be important, the mother wave amplitude must be large enough to trigger the coalescence quickly so that the nonlinear evolution can mature within the plasma formation time τ_p . The mother waves are pumped by the lithium ions created by photoionization of the released neutral lithium atoms. As explained in section 2, the rate of creation of the lithium ions is given by $\tau_p^{-1} \sim 1/165 \text{ s}^{-1}$. Since the energy per newborn lithium ion is $m_{Li}V_s^2/2$, the rate at which the released energy goes into the generation of the mother waves is $(n_{Li}^{Total} m_{Li} V_s^2 / 2 \tau_p)$. The coalescence is triggered when this rate equals the rate of production of the daughter waves as given in equation (25),

$$\frac{n_{Li}^{Total} m_{Li} V_s^2}{2\tau_p} \approx \omega_3 \frac{m_H}{m_e} \frac{\omega_3^4}{\Omega_H^4} \frac{W_1^2}{(B_0^2/8\pi)}. \quad (27)$$

This indicates that the necessary condition for the onset of the coalescence process is

$$\frac{W_1}{n_{Li}^{Total} m_{Li} V_s^2 / 2} \sim \left(\frac{1}{\Omega_H \tau_p} \frac{m_e}{m_H} \left(\frac{\Omega_H}{\omega_3} \right)^5 \frac{B_0^2}{4\pi n_{Li}^{Total} m_{Li} V_s^2} \right)^{1/2}. \quad (28)$$

For $L = 2$ parameters, $n_{Li}^{Total} = 300/\text{cc}$, $\tau_p \sim 165 \text{ s}$, $B_0^2/4\pi n_{Li} m_{Li} V_s^2 \approx 4 \times 10^4$, and $\omega_3/\Omega_H \sim 1$, we see that the value of the ratio $W_1/(n_{Li}^{Total} m_{Li} V_s^2 / 2)$ is approximately 0.03. This implies that with only a small fraction of the released energy delivered into the mother waves, it is sufficient to trigger the generation of the coalescence process at $t = 0.03\tau_p \sim 1.5 \text{ s}$. This is almost instantaneous and hence will allow the nonlinear process to comfortably evolve and mature within the plasma formation time. In the following section, we examine the ability of the daughter waves to meet the resonance condition and enable pitch angle scattering of the energetic electrons.

4. Resonance Criterion

[30] For successful pitch angle scattering, we must ensure that the wave vectors generated are consistent with the resonance condition,

$$\omega - k_z v_z - \Omega_e/\gamma_R = 0, \quad (29)$$

where $\gamma_R = 1/\sqrt{1 - (v/c)^2} = 2E + 1$ is the relativistic factor with electron rest energy taken to be 0.5 MeV, and E is the electron kinetic energy in MeV. Because of the coalescence condition, the daughter shear Alfvén waves are generated with $\bar{k}_z \sim 1$. Once the energy is transferred to the daughter waves, they are distributed among all possible wave vectors. Because of magnetic beaching effect [Stix, 1992], these wave vectors can assume larger numbers as the waves propagate toward the equator. A rough estimate indicates that largest value of $\bar{k}_z \sim (4\beta_H)^{-1/6}$ is possible before the waves are cyclotron damped. This implies that $\bar{k}_{z,max} \sim 5$ because at $L = 2$, the magnitude of $\beta_H \sim 10^{-5}$. Since relativistic electron speed along the magnetic field is $v_z \approx c \cos\theta$ and $\omega \ll \Omega_e/\gamma_R \sim k_z v_z$, the resonance condition equation (29) can be expressed as

$$\frac{k_z c}{\omega_{pH}} \cos\theta \approx \frac{(\Omega_e/\omega_{pH})}{2E (MeV) + 1}. \quad (30)$$

Since $\Omega_e/\omega_{pH} \sim 17$ at $L = 2$, the right-hand side of equation (30) is approximately 3 for a 2-MeV electron. Thus the spectrum of parallel wave vectors generated can meet the resonance condition for a wide range of energies.

5. Pitch Angle Scattering of Relativistic Electrons by Daughter Waves

[31] The general theory of pitch angle scattering of relativistic electrons has been extensively studied [Lyons *et al.*, 1971, 1972; Lyons, 1974]. The turbulence generated by the whistler or the EMIC waves have been considered as the source for inducing pitch angle scattering of the trapped relativistic electrons in the radiation belt environment. In the method we propose in this article, the scattering will be induced by the turbulence generated by shear Alfvén waves seeded by the release of neutral gas in the radiation belt. These shear Alfvén waves are linearly polarized because of coupling of the left and right circularly polarized normal modes in the frequency range near the ion cyclotron frequency because $k_{\perp} > k_z$. In this respect, they are different from left circularly polarized EMIC modes that have been considered for pitch angle scattering.

[32] The turbulence is generated by waves in cold predominantly hydrogen plasma, which is described by the dispersion relation equation (14) whose solution is given in equation (15). In section 4, we saw that nonlinear coalescence can result into shear Alfvén waves with $k_{\perp} > k_z$ but $k_{\perp}(m_e/m_H)^{1/2} \ll k_z$. The wave magnetic field is given by

$$B_{1y} = 2^{-1/2} \sum_k B_{k,y} \exp(-i\omega t + ik_z z + ik_{\perp} r_{\perp}) + c.c. \quad (31)$$

Because the magnetic fluctuations are quasi-static $\omega \sim \Omega_H \ll \Omega_e (= \Omega_e/\gamma_R)$, the energy of the relativistic electron does not change, and hence we do not consider energy diffusion. In addition, for Alfvénic waves, it can be shown from the general quasi-linear equation that diffusion of v_z and v_{\perp} are similar in magnitude, i.e., $D_{zz} \sim D_{\perp\perp} \sim D_{\perp z}$ but with different pitch angle dependence. For particles whose pitch angle is close to $\pi/2$, the v_z diffusion will dominate, whereas for those whose pitch angle is close to 0, the v_{\perp} diffusion will dominate. Since trapped particles have large pitch angles, we are primarily

interested in the v_z diffusion. The $\vec{v} \times \vec{b}_1$ force changes the electron velocity in the z direction, and hence its pitch angle θ , since $v_z = v \cos \theta$ and $\delta v_z = -v \sin \theta \delta \theta$ when expressed in cylindrical coordinates. This results in a slow change in the pitch angle distribution $f_0(\theta)$ approximately given in spherical coordinates by

$$\frac{\partial f_0(\theta)}{\partial t} = \frac{1}{\sin \theta} \frac{\partial}{\partial \theta} \sin \theta D_{\theta\theta} \frac{\partial f_0(\theta)}{\partial \theta}. \quad (32)$$

We calculate the diffusion coefficient in cylindrical coordinates because of physical transparency, and then transforming in spherical coordinates, we express

$$D_{zz} = \left\langle a_{1z}^* \delta v_{z1} + a_{1z} \delta v_{z1}^* \right\rangle \approx v^2 D_{\theta\theta} / 2. \quad (33)$$

Here a_{1z} and $\delta v_{z1} = \int a_{1z} dt$ are acceleration and change in electron velocity in the z direction, respectively, as the electron interacts with the resonant wave, and $\langle f(t) \rangle \equiv (1/T_0) \int f(t) dt$, where T_0 is a time interval that is much larger than the period of the fast oscillation, implies fast time averaging. In the quasi-linear theory, the particles interact with individual waves, which in our case are plane waves. The net modification to the equilibrium distribution due to an ensemble of waves constitutes the quasi-linear effect. We examine the interaction of shear Alfvén waves with wave vectors in the (x, z) plane and then integrate over an ensemble of all amplitudes and directions of the wave vectors to obtain the net quasi-linear diffusion. The z component of the equation of motion for the resonant relativistic electron in a magnetic field is

$$a_{1z} = \frac{dv_{1z}}{dt} = \frac{e}{m_e \gamma_R c} v_x B_{1,y}(z), \quad (34)$$

where $d\gamma_R/dt$ is neglected because of conservation of energy. The unperturbed orbits of the electrons are

$$\begin{aligned} z &= v_z t, & v_x &= v_\perp \cos \bar{\Omega}_e t, & v_y &= v_\perp \sin \bar{\Omega}_e t, \\ x &= (v_\perp / \bar{\Omega}_e) \sin \bar{\Omega}_e t. \end{aligned} \quad (35)$$

Substituting v_x , x , and z in equation (34) and using a Fourier component of the magnetic field, i.e., $B_{1,y} = 2^{-1/2} B_{k,y} \exp(-i\omega t + ik_z z + ik_\perp r_\perp)$, we obtain the perturbed equation of motion along the magnetic field B_{0z} ,

$$a_{1kz} = \frac{e}{\sqrt{2} m_e \gamma_R c} v_\perp B_{k,y} \sum_{n=-\infty}^{\infty} \frac{n J_n(\bar{\sigma})}{\bar{\sigma}} \exp(-i\omega t + ik_z v_z t + in \bar{\Omega}_e t), \quad (36)$$

where $\bar{\sigma} = k_x v_\perp / \bar{\Omega}_e \equiv k_\perp v_\perp / \bar{\Omega}_e$.

[33] Now we calculate change of v_{1z} . Since the magnetic fluctuations are quasi-static, we ignore ω and consider resonance with only the $n = \pm 1$ electron harmonics. Thus δv_{1z} is given by

$$\delta v_{1kz} = \frac{e}{\sqrt{2} m_e \gamma_R c} v_\perp B_{k,y} \frac{J_{\pm 1}(\bar{\sigma})}{\bar{\sigma}} \int_{-\infty}^{\tau} dt \exp(ik_z v_z t \pm i \bar{\Omega}_e t). \quad (37)$$

By integrating equation (37), we get

$$\delta v_{1kz} = \frac{e}{\sqrt{2} m_e \gamma_R c} v_\perp \frac{J_{\pm 1}(\bar{\sigma})}{\bar{\sigma}} B_{k,y} \frac{1}{i(\pm \bar{\Omega}_e + k_z v_z)} \times \exp i(\pm \bar{\Omega}_e + k_z v_z) t. \quad (38)$$

Using equations (36) and (38) in equation (33) and summing over the k spectrum, we obtain D_{zz} ,

$$\begin{aligned} D_{zz}(v_z) &= (e/m_e \gamma_R c)^2 v_\perp^2 \sum_{\vec{k}} \left| \vec{B}_k \times \vec{k} / k \right|^2 \left[\frac{J_{\pm 1}(\bar{\sigma})}{\bar{\sigma}} \right]^2 \pi \delta(k_z v_z \pm \bar{\Omega}_e) \\ &\approx \pi \bar{\Omega}_e v_\perp^2 |B_1(|k_z| = \bar{\Omega}_e/c)|^2 / 4B_0^2, \end{aligned} \quad (39)$$

where $J_{\pm 1}(\bar{\sigma})/\bar{\sigma} \approx \pm 1/2$ since $\bar{\sigma}$ is small.

[34] We estimate the change in pitch angle as

$$\Delta \theta^2 \approx T_{Res} D_{\theta\theta} \approx 2 T_{Res} D_{zz} / v^2 \approx \pi \bar{\Omega}_e T_{Res} |B_1|^2 / 2B_0^2, \quad (40)$$

where T_{Res} is the residence time of the electron inside the turbulent cloud with dimensions L_z and L_ϕ , along the magnetic field and in the azimuthal direction, respectively.

[35] The electron trajectory consists of a bounce motion along the magnetic field as well as an azimuthal drift. The bounce time of a typical relativistic electron is $T_B \sim \pi L R_E / c$ seconds. (Actually, T_B is considerably smaller depending on the pitch angle because of mirroring.) During one bounce, the relativistic electron will be resident inside the cloud for L_z/c seconds. During the lifetime of the turbulence T_t , the electron enters the plasma cloud $N_c = T_t V_\phi / 2\pi L R_E$ times while it encircles the earth with an azimuthal velocity $V_\phi \approx c \rho_e / L R_E$ [Hargreaves, 1992] where ρ_e is the electron gyro-radius. The number of bounce while azimuthally drifting inside the plasma cloud is $N_B = L_\phi / V_\phi T_B$. A relativistic electron resides inside the cloud during the turbulence lifetime for T_{Res} seconds, where

$$T_{Res} = N_B N_c L_z / c = \frac{T_t}{2\pi^2 (L R_E)^2} L_z L_\phi. \quad (41)$$

More accurately, for a mirroring 2-MeV electron with 45° pitch angle, it can be shown that $T_B = 1.7 R_E / c$, which makes T_{Res} about 4 times larger. Taking this into account and substituting equation (41) in equation (40), we get

$$\Delta \theta^2(\gamma_R) = \frac{4L \bar{\Omega}_e T_t}{4\pi (B_0^2/8\pi) (L R_E)^3} \frac{W_3 L_z L_\phi R_E}{1 + \bar{\Omega}_e^2 / \omega_{pH}^2} \frac{2\Delta L_z(\gamma_R)}{L_z}, \quad (42)$$

where W_3 is the energy density of the daughter waves and $2\Delta L_z(\gamma_R)/L_z$ is the fraction of electron trajectory over which the resonance condition is satisfied. ΔL_z corresponds to a change of $\Delta \bar{k}_z$ such that the resonance condition is satisfied for every \bar{k}_z in the interval $[\bar{k}_z + \Delta \bar{k}_z, \bar{k}_z - \Delta \bar{k}_z]$.

[36] From equation (42), it can be seen that the change in the pitch angle depends on the energy deposited into the daughter waves and the turbulence lifetime but not on turbulent energy distribution in space. The factor $(1 + \bar{\Omega}_e^2 / \omega_{pH}^2)^{-1}$ appears in equation (42) because the magnetic part of the wave energy density is less by a factor $(1 + \bar{k}_z^2 c^2 / \omega_{pH}^2) = (1 + \bar{\Omega}_e^2 / \omega_{pH}^2)$ than the total wave energy

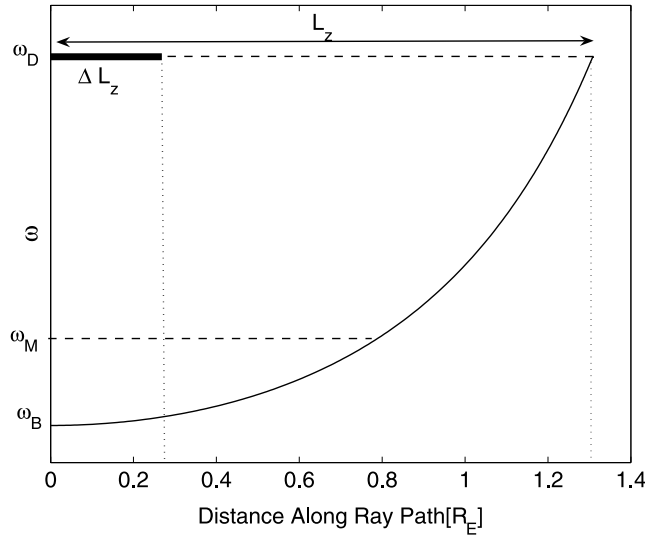


Figure 5. Mother waves generated near the third lithium cyclotron harmonic, $\omega_M \sim 3\Omega_{Li}$, and daughter waves with $\omega_D \sim 2\omega_M$ undergo reflection when their frequencies approach the hydrogen-helium Buchsbaum frequency ω_B . In this example, daughter waves travel a distance L_z from the equator before reflection, approximately twice as far as the mother waves. The daughter wave with $\bar{k}_z = 4$ initially will reach $\bar{k}_z = 2$, after a distance indicated by ΔL_z beyond which they are no longer resonant with a 2-MeV electron. $\Delta L_z/L_z \approx 0.25$.

density W_3 [see equation (A35)], where we have used the resonance condition $\bar{\Omega}_e \leq k_z c$.

[37] At $L = 2$ using $B_0 = 0.04$ G and the release of 10^{29} lithium atoms with kinetic energy 1.75 eV, we have

$$\Delta\theta^2(\gamma_R) \approx \gamma_R^{-1} \frac{T_i \eta}{1 + \bar{\Omega}_e^2 / \omega_{pH}^2} \frac{2\Delta L_z(\gamma_R)}{L_z}, \quad (43)$$

where η is the fraction of energy released which goes into the long wavelength part of the turbulence.

[38] The helium-hydrogen collisions will lead to damping of the waves at the rate of $0.5\nu_{H-He} = 0.5 \times 10^{-3} \text{ s}^{-1}$. Hydrogen-electron collisions could also be important and will be addressed in a subsequent article. Although waves are generated continuously over the ionization time $T_i = 3000$ s, we use the turbulence lifetime $T_t = 2000$ s. For 2-MeV electrons, $\gamma_R = 5$. With $\bar{\Omega}_e^2 / \omega_{pH}^2 \sim 9$ and $\Delta L_z(\gamma_R)/L_z \sim 1/4$ (see Figure 5), we get

$$\Delta\theta^2 \approx 20\eta. \quad (44)$$

Thus with a small fraction (few percent) of the released energy deposited into the turbulence, a change in pitch angle of order unity can be achieved. This is large enough to scatter the trapped relativistic electrons into the loss cone.

[39] From the above, it is clear that for electron energy above megaelectron volts, quasi-linear scattering is quite efficient. As noted earlier, the turbulence generated by neutral gas release is intense and may give rise to randomly distributed magnetic structures. This is a major departure from the quasi-linear picture where the wave magnetic field is assumed to be plane waves which are periodic. Such magnetic structures offer the possibility of inducing pitch

angle scattering even in those electrons that are not quite in resonance. This will enhance the scattering rate and will be especially important for electrons with energies less than megaelectron volts. The theory for nonresonant scattering is now under development.

6. Conclusion

[40] We have shown that it is possible to use a neutral gas release as a source for intense electromagnetic turbulence in a low- β near-Earth plasma. An essential ingredient for the success of this process is the ability to create a ring distribution in the perpendicular velocity of the injected ions. This converts the orbital kinetic energy of the neutrals into a reservoir of free energy for the waves to tap into. Since the orbital kinetic energy is large, it allows for a very large source of energy for exploitation. It is equivalent to creating an ion magnetron in the radiation belt and maintaining it by photoionization. The magnetron utilizes the free energy to amplify the necessary electromagnetic waves for pitch angle scattering. The proximity to the Earth will allow relatively easy diagnosis of the nonlinear evolution which will help clarify the nonlinear plasma dynamics in the near-Earth environment.

[41] In this article, we have focused on only the plasma physics aspects. There are a number of technical issues related to the release of such a large amount of matter. We have considered some of them, but a more detailed analysis will be necessary. It is found that vaporization of a ton of lithium (without formation of oxides) can be achieved by 9 tons of a gasless thermal driver such as titanium-boron (Ti/2B; P. Zavitsanos, private communication). Transportation of this amount of material into space may present technical challenges. However, it is to be noted that the NASA/Combined Release and Radiation Effects Satellite (CRRES) is comparable to our specification and can be modified for the release of larger amount of materials. Thus existing and proven technology may be sufficient to conduct an experiment to test the concept we suggest. However, the possibility for a more efficient method for vaporization that can yield more energy for less mass is discussed in Appendix C.

[42] While this study establishes the possibility of neutral gas release as a means for seeding and probing nonlinear processes in the near-Earth plasma, a more detailed theoretical/computational/experimental program is currently underway for a more quantitative analysis. Detailed analytical and numerical studies to investigate the quasi-linear and nonlinear characteristics such as the magnitude of the saturated wave amplitude generated by the instability, transport of energy in the turbulence, and the efficiency of pitch angle scattering of the relativistic electrons, etc., are now under investigation.

Appendix A: Shear Alfvén Waves Around Ion Cyclotron Frequency

A1. Linear Dispersion Relation

[43] In a neutral gas release experiment considered in this article, the plasma generated will consist predominantly of hydrogen (H) and electron (e) with about 5% lithium (Li). At $L = 2$, helium is also present but with low abundance of about 5% of H^+ [Craven *et al.*, 1997]. The lithium ion ring distribution generated by the shaped release of neutral

lithium gas perpendicular to the ambient magnetic field will give rise to shear Alfvén waves near the lithium cyclotron frequency with electric field fluctuations predominantly perpendicular to the magnetic field. Initially, there is no thermal lithium component, but after a few lithium-hydrogen collision time, a thermal lithium component will be generated. Considering $k_y = 0$ and $k_z \ll k_x \sim k$, the dispersion relation is determined by Maxwell equations neglecting the displacement current,

$$\nabla \times \vec{B} = \frac{4\pi}{c} \vec{J}, \quad (\text{A1})$$

$$\nabla \times \vec{E} = -\frac{1}{c} \frac{\partial \vec{B}}{\partial t}, \quad (\text{A2})$$

along with the quasi-neutrality condition

$$\nabla \cdot \vec{J} = 0, \quad (\text{A3})$$

where $\vec{J} = \vec{\sigma} \cdot \vec{E}$ and $\vec{\sigma}$ is the conductivity tensor. Equations (A1) and (A2) lead to

$$(k_x^2 + k_z^2) \vec{E} - \vec{k}(k_x E_x + k_z E_z) = \frac{4\pi i \omega}{c^2} \vec{J}. \quad (\text{A4})$$

From the y component of equation (A4), we find that

$$E_y = \frac{4\pi i \omega \sigma_{yx}}{k^2 c^2 \left(1 - \frac{4\pi i \omega}{c^2} \frac{\sigma_{yy}}{k^2}\right)} E_x \approx i \frac{\omega_{pH}^2}{k^2 c^2} \frac{\omega}{\Omega_H} E_x, \quad (\text{A5})$$

and from the quasi-neutrality condition, we obtain

$$E_z = -\frac{\sigma_{xx}}{\sigma_{zz}} \frac{k_x}{k_z} E_x. \quad (\text{A6})$$

Using equations (A5) and (A6) in the x component of equation (A4), we obtain the dispersion relation for the shear Alfvén waves with $k_x \gg \omega_{pH}/c > k_z$,

$$\frac{k_z^2 c^2}{\omega^2} = \frac{4\pi i}{\omega} \sigma_{xx} \left(1 - \frac{k_x^2 c^2}{4\pi i \omega \sigma_{zz}}\right), \quad (\text{A7})$$

where the conductivities σ_{xx} and σ_{zz} are defined as

$$\begin{aligned} \sigma_{xx} = & -\frac{i}{2} \sum_{\alpha} \omega_{p\alpha}^2 \sum_l \int_{-\infty}^{\infty} dv_z \int_0^{\infty} dv_{\perp}^2 \left(\left(1 - \frac{k_z v_z}{\omega}\right) \right. \\ & \cdot \frac{\partial f_{0\alpha}}{\partial v_{\perp}^2} + \frac{k_z v_z}{\omega} \frac{\partial f_{0\alpha}}{\partial v_z^2} \left. \right) \frac{(l\Omega_{\alpha}/k_{\perp})^2 J_l^2(\sigma_{\alpha})}{\omega - k_z v_z - l\Omega_{\alpha}}, \end{aligned} \quad (\text{A8})$$

$$\begin{aligned} \sigma_{zz} = & -\frac{i}{2} \sum_{\alpha} \omega_{p\alpha}^2 \sum_l \int_{-\infty}^{\infty} dv_z \int_0^{\infty} dv_{\perp}^2 \left(\frac{\partial f_{0\alpha}}{\partial v_z^2} - \frac{l\Omega_{\alpha}}{\omega} \right. \\ & \cdot \left. \left(\frac{\partial}{\partial v_z^2} - \frac{\partial}{\partial v_{\perp}^2} \right) f_{0\alpha} \right) \frac{v_z^2 J_l^2(\sigma_{\alpha})}{\omega - k_z v_z - l\Omega_{\alpha}}, \end{aligned} \quad (\text{A9})$$

and $f_{0\alpha}$ is the equilibrium distribution function, $\omega_{p\alpha}$ is the plasma frequency, Ω_{α} is the cyclotron frequency, $\sigma_{\alpha} =$

$k_{\perp} v_{\perp} / \Omega_{\alpha}$ where α represents the species, and $J_l(\sigma)$ are the Bessel functions. Also, note that σ_{xx} is due to perpendicular motion of ions for $\omega \ll \Omega_e$, whereas σ_{zz} leads to parallel motion which is dominated by the electrons because of their larger mobility. Hence σ_{zz} may be simplified by neglecting the ion contribution and assuming $l=0$ and $\sigma_e = k_{\perp} v_{\perp} / \Omega_e \ll 1$, so that

$$\sigma_{zz} = -i\omega_{pe}^2 \int_{-\infty}^{\infty} dv_z \int_0^{\infty} v_{\perp} dv_{\perp} \frac{v_z^2}{\omega - k_z v_z} \frac{\partial f_{0e}}{\partial v_z^2}. \quad (\text{A10})$$

The electron and the thermal components of the magnetosphere (for example, hydrogen, helium, lithium when thermalized, etc.) are represented by Maxwellian distribution function,

$$f_{0\alpha} = \left(\frac{1}{\pi v_{t\alpha}^2}\right)^{3/2} \exp\left(-\frac{v_{\perp}^2}{v_{t\alpha}^2}\right) \exp\left(-\frac{v_z^2}{v_{t\alpha}^2}\right). \quad (\text{A11})$$

where $v_{t\alpha} = \sqrt{2T_{\alpha}/m_{\alpha}}$ is the thermal velocity. The initial lithium distribution function is a narrow ring distribution, such as given in equation (2). For $V_s \gg v_{tLi}$, the perpendicular velocity distribution may be replaced by a delta function so that

$$f_{0Li} = \frac{1}{(2\pi)^{3/2} V_s v_{tLi}} \delta(v_{\perp} - V_s) \exp\left(-\frac{v_z^2}{v_{tLi}^2}\right). \quad (\text{A12})$$

Using equations (A11) and (A12) in equation (A8), we calculate $\sigma_{xx} = \sum_{\alpha} \sigma_{xx}^{\alpha} + \sigma_{xx}^{Li}$ where α denotes the thermal population. It can be shown that

$$\sigma_{xx}^{\alpha} = -\frac{i\omega_{p\alpha}^2}{4\pi\omega} \left[\sum_l l^2 \frac{\Gamma_l(b_{\alpha})}{b_{\alpha}} \left(\frac{\omega}{k_z v_{t\alpha}}\right) Z\left(\frac{\omega - l\Omega_{\alpha}}{k_z v_{t\alpha}}\right) \right], \quad (\text{A13})$$

where $b_{\alpha} = (k_x \rho_{\alpha})^2$, $\rho_{\alpha} = v_{t\alpha} / \Omega_{\alpha}$, $Z(\zeta)$ is the plasma dispersion function, and $\Gamma_l(b) = I_l(b) \exp(-b)$, where $I_l(b)$ are the modified Bessel function. Similarly, the lithium ring distribution leads to

$$\begin{aligned} \sigma_{xx}^{Li} = & \frac{i\omega_{pLi}^2}{4\pi\omega} \sum_l \left(\frac{l\Omega_{Li}}{k_{\perp}}\right)^2 \left[\left(\frac{2J_l^2(\sigma_s)}{v_{tLi}^2} - \frac{1}{V_s} \frac{dJ_l^2(\sigma_s)}{dV_s}\right) \right. \\ & \cdot \left. \left(\frac{1}{2} Z'\left(\frac{\omega - l\Omega_{Li}}{k_z v_{tLi}}\right)\right) - \frac{1}{V_s} \frac{dJ_l^2(\sigma_s)}{dV_s} \left(\frac{\omega}{k_z v_{tLi}}\right) \right. \\ & \cdot \left. Z\left(\frac{\omega - l\Omega_{Li}}{k_z v_{tLi}}\right) \right], \end{aligned} \quad (\text{A14})$$

where $\sigma_s = k_{\perp} V_s / \Omega_{Li}$ and $Z' = dZ(\zeta)/d\zeta$. Also, using equation (A11) in equation (A10), we find that

$$\sigma_{zz} = \frac{i}{4\pi} \frac{\omega_{pe}^2}{\omega} \zeta^2 Z'(\zeta), \quad (\text{A15})$$

where $\zeta = \omega / k_z v_{te}$.

[44] Substituting equations (A13)–(A15) in equation (A7), we derive the general dispersion relation,

$$\begin{aligned} \frac{k_z^2 c^2}{\omega^2} \left(1 + \frac{k_x^2 c^2}{\omega_{pe}^2 \zeta^2 Z'(\zeta)} \right)^{-1} &= \sum_{\alpha} \frac{\omega_{p\alpha}^2}{\omega^2} \sum_l l^2 \frac{\Gamma_l(b_{\alpha})}{b_{\alpha}} \zeta_{\alpha} Z(\zeta_{\alpha}^l) \\ &\quad - \frac{\omega_{pLi}^2}{\omega^2} \sum_l \left(\frac{l\Omega_{Li}}{k_{\perp}} \right)^2 \left[\left(\frac{2J_l^2(\sigma_s)}{v_{Li}^2} \right. \right. \\ &\quad \left. \left. - \frac{1}{V_s} \frac{dJ_l^2(\sigma_s)}{dV_s} \right) \frac{Z'(\zeta_{Li}^l)}{2} \right. \\ &\quad \left. - \frac{1}{V_s} \frac{dJ_l^2(\sigma_s)}{dV_s} \zeta_{Li} Z(\zeta_{Li}^l) \right], \end{aligned} \quad (\text{A16})$$

where $\zeta_{\alpha} = (\omega/k_z v_{t\alpha})$ and $\zeta_{\alpha}^l = (\omega - l\Omega_{\alpha})/k_z v_{t\alpha}$.

[45] The phase speed of the waves are comparable to the Alfvén speed and hence much larger than the thermal speed of any species, i.e., $\omega - l\Omega_{\alpha} \gg k_z v_{t\alpha}$. Hence the Z functions can be expanded for large arguments. Noting that $\Gamma_l = \Gamma_{-l}$, equation (A13) reduces to

$$\sigma_{xx}^{\alpha} = \frac{i\omega}{4\pi} \sum_l \frac{l^2 \omega_{p\alpha}^2}{\omega^2 - l^2 \Omega_{\alpha}^2} \frac{2\Gamma_l(b_{\alpha})}{b_{\alpha}}. \quad (\text{A17})$$

Similarly, equation (A14) reduces to

$$\begin{aligned} \sigma_{xx}^{Li} &= -\frac{\omega_{pLi}^2}{\omega^2} \sum_l l^2 \\ &\quad \times \left[\frac{1}{\sigma_s} \frac{dJ_l^2(\sigma_s)}{d\sigma_s} \left(\frac{\omega}{\omega - l\Omega_{Li}} \right) + \frac{J_l^2(\sigma_s)}{\sigma_s^2} \left(\frac{k_z V_s}{\omega - l\Omega_{Li}} \right)^2 \right], \end{aligned} \quad (\text{A18})$$

where $l < m_{Li}/m_H$ for the lithium component so that hydrogen cyclotron harmonic resonance is avoided. The second term in equation (A18) is proportional to $(V_s/V_A)^2$ which for our application is $\sim 10^{-4}$. Hence we ignore this term. However, for $V_s/V_A > 1$, a condition often reached in the solar wind-comet interaction, this term can be dominant and give rise to low-frequency Alfvénic waves with $k_z \gg k_{\perp}$ [Sharma and Patel, 1986; Galeev and Sagdeev, 1988]. From equations (A17) and (A18), we obtain simplified σ_{xx} ,

$$\begin{aligned} \sigma_{xx} &= -\frac{i\omega}{4\pi} \left[\sum_{\alpha,l} \frac{l^2 \omega_{p\alpha}^2}{l^2 \Omega_{\alpha}^2 - \omega^2} \frac{2\Gamma_l(b_{\alpha})}{b_{\alpha}} \right. \\ &\quad \left. - \omega_{pLi}^2 \sum_l \frac{1}{\sigma_s} \frac{dJ_l^2(\sigma_s)}{d\sigma_s} \frac{l^2}{\omega(\omega - l\Omega_{Li})} \right]. \end{aligned} \quad (\text{A19})$$

Using equations (A15) and (A19) in equation (A7), the simplified dispersion relation for the shear Alfvén waves is

$$\begin{aligned} D(\omega, k) &= \frac{k_z^2 V_A^2}{\omega^2} \left(1 + \frac{k_x^2 c^2}{\omega_{pe}^2 \zeta^2 Z'(\zeta)} \right)^{-1} \\ &\quad - \sum_{\alpha,l} \frac{n_{\alpha} m_{\alpha}}{n_H m_H} \frac{l^2 \Omega_{\alpha}^2}{l^2 \Omega_{\alpha}^2 - \omega^2} \frac{2\Gamma_l(b_{\alpha})}{b_{\alpha}} \\ &\quad + \sum_l \frac{n_{Li} m_{Li}}{n_H m_H} \frac{dJ_l^2(\sigma_s)}{\sigma_s d\sigma_s} \frac{l^2 \Omega_{Li}^2}{\omega(\omega - l\Omega_{Li})} = 0. \end{aligned} \quad (\text{A20})$$

The last term is due to the lithium ions just after ionization with ring distribution. This term is responsible for the

instability. The contribution of the thermal lithium, which may be subsequently generated because of lithium-hydrogen collision, is included in the second term. The thermal lithium contribution can lead to a threshold condition for the instability. Combining the thermal and ring lithium terms, we rewrite equation (A20) as

$$\begin{aligned} D(\omega, k) &= \frac{k_z^2 V_A^2}{\omega^2} \left(1 + \frac{k_x^2 c^2}{\omega_{pe}^2 \zeta^2 Z'(\zeta)} \right)^{-1} \\ &\quad - \sum_{\alpha,l} \frac{n_{\alpha} m_{\alpha}}{n_H m_H} \frac{l^2 \Omega_{\alpha}^2}{l^2 \Omega_{\alpha}^2 - \omega^2} \frac{2\Gamma_l(b_{\alpha})}{b_{\alpha}} \\ &\quad + \sum_l \frac{n_{Li} m_{Li}}{n_H m_H} \frac{dJ_l^2(\sigma_s)}{\sigma_s d\sigma_s} \frac{l^2 \Omega_{Li}^2}{\omega(\omega - l\Omega_{Li})} \\ &\quad \cdot \left(1 + \frac{n_{Li}}{n_{Li}} \frac{2\Gamma_l(b_{Li})}{b_{Li}} \frac{1}{(dJ_l^2(\sigma_s)/\sigma_s d\sigma_s)} \right) = 0, \end{aligned} \quad (\text{A21})$$

where the subscript ‘‘Lit’’ represents thermalized lithium quantities, and the subscript ‘‘ α ’’ represents the natural ambient species. Equation (A21) indicates that, initially, there is no threshold for the instability, but as the thermal lithium population increases, there is a threshold determined by the condition

$$\frac{n_{Li}}{n_{Li}} \frac{2\Gamma_l(b_{Li})}{b_{Li}} \frac{1}{|dJ_l^2(\sigma_s)/\sigma_s d\sigma_s|} = 1. \quad (\text{A22})$$

A2. Wave Energy Density

[46] We now examine the wave energy. To do this, we introduce the vector potential \vec{A} such that $\vec{B} = \nabla \times \vec{A}$. Using the Coulomb gauge, i.e., $\nabla \cdot \vec{A} = ik_x A_x + ik_z A_z = 0$, and since $k_y = 0$, $A_x = -A_z k_z/k_x$, and we get for the shear Alfvén waves of interest

$$B_y = -ik_x A_z + ik_z A_x = -ik_x A_z (1 + k_z^2/k_x^2) \cong -ik_x A_z, \quad (\text{A23})$$

where $k_x \gg k_z$ is assumed. In addition,

$$E_x = -ik_x \phi - \partial A_x / c \partial t \cong -ik_x \phi, \quad (\text{A24})$$

$$E_z = -\partial \phi / \partial z - \partial A_z / c \partial t, \quad (\text{A25})$$

$$j_z = \frac{c}{4\pi} k_{\perp}^2 A_z = \sigma_{zz} E_z = i \frac{\omega_{pe}^2}{4\pi \omega} (-\partial \phi / \partial z - \partial A_z / c \partial t). \quad (\text{A26})$$

From equation (A26), we can solve for the electrostatic potential

$$\phi = A_z \frac{\omega}{k_z c} \left(1 + \frac{k_x^2 c^2}{\omega_{pe}^2} \right). \quad (\text{A27})$$

For the parameter range of our interest, i.e., $b_H \ll 1$, the dispersion relation equation (6) reduces to

$$\omega_r = k_z V_A \left(1 + \frac{k_x^2 c^2}{\omega_{pe}^2} + \frac{k_z^2 c^2}{\omega_{pH}^2} \right)^{-1/2}. \quad (\text{A28})$$

Substituting equation (A28) in equation (A27), we obtain

$$\varphi = \frac{V_A}{c} \left(1 + \frac{k_x^2 c^2}{\omega_{pe}^2} \right) \left(1 + \frac{k_x^2 c^2}{\omega_{pe}^2} + \frac{k_z^2 c^2}{\omega_{pH}^2} \right)^{-1/2} A_z, \quad (\text{A29})$$

From equations (A25) and (A27), we get

$$E_z = -i \frac{\omega}{c} \frac{k_x^2 c^2}{\omega_{pe}^2} A_z. \quad (\text{A30})$$

The energy of the wave is distributed into kinetic energy of the particles (i.e., electrons and hydrogen) and field fluctuations. Thus the time-averaged wave energy density is

$$W = \frac{1}{2} \left(\frac{1}{2} m_H n_H |v_H|^2 + \frac{1}{2} m_e n_e \left| \frac{e E_z}{m_e \omega} \right|^2 + \frac{|B_y|^2}{8\pi} \right), \quad (\text{A31})$$

where v_H is the hydrogen perturbed velocity given by

$$\vec{v}_H = \frac{c}{B_0} \left(\frac{\Omega_H^2 \vec{E} \times \hat{b} - i \omega \Omega_H \vec{E}}{\Omega_H^2 - \omega^2} \right). \quad (\text{A32})$$

[47] For the parameters corresponding to the mother waves discussed in section 2.3, $k_x^2 c^2 / \omega_{pe}^2 \gg k_z^2 c^2 / \omega_{pH}^2$ and $\omega < \Omega_H$ so that the drift approximation for the hydrogen, i.e. $v_H \approx -c \nabla_{\perp} \phi / B$, can be used. Substituting for φ , E_z , and B_y from equations (A29), (A30), and (A23) in equation (31), we get

$$W = \frac{|B_y|^2}{8\pi} \left(1 + \frac{k_x^2 c^2}{\omega_{pe}^2} \right). \quad (\text{A33})$$

[48] For the parameters corresponding to the daughter waves discussed in section 3, $k_x^2 c^2 / \omega_{pe}^2 \ll k_z^2 c^2 / \omega_{pH}^2$ and $\omega \sim \Omega_H$. Hence v_H cannot be simplified. In this limit, E_z is negligible and the wave dispersion relation is given by

$$\omega_r = k_z V_A \left(1 + \frac{k_z^2 c^2}{\omega_{pH}^2} \right)^{-1/2}. \quad (\text{A34})$$

Following similar algebra, it can be shown that the wave energy density in this limit is

$$W = \frac{|B_y|^2}{8\pi} \left(1 + \frac{k_z^2 c^2}{\omega_{pH}^2} \right). \quad (\text{A35})$$

Appendix B: Calculation of the Second-Order Current and Energy Transfer Rates

B1. Second-Order Current

[49] Here we calculate the nonlinear second-order current for small amplitude oscillations (i.e., $\vec{v}_{\perp} \ll \omega / k_{\perp}$). The nonlinear current induces a second-order electric field $E^{(2)}$. We consider the interaction of two short wavelength

mother waves capable of generating a long wavelength daughter wave in accordance to the decay law described in equations (18) and (19). The wave vectors of the mother waves are along the x axis. The electric and magnetic fluctuations associated with the linear and nonlinear currents due to ion motion generated by the interaction of mother waves define the daughter waves, and their relationship is given in equation (24).

[50] The nonlinear current $j_x^{(2)}$ can be obtained from the plasma momentum balance equation,

$$nm_H \left(\frac{\partial \vec{v}}{\partial t} + (\vec{v} \cdot \nabla) \vec{v} \right) = c^{-1} \vec{j} \times \vec{B}. \quad (\text{B1})$$

Using the continuity equation, we can rewrite equation (B1) as

$$m_H \frac{\partial}{\partial t} \left(n^{(1)} \vec{v}^{(1)} + n_0 \vec{v}^{(2)} \right) + m_H \nabla_i \left(n_0 \vec{v}_i^{(1)} \vec{v}^{(1)} \right) = c^{-1} \vec{j}^{(2)} \times \vec{B}_0 + c^{-1} \vec{j}^{(1)} \times \vec{B}^{(1)}. \quad (\text{B2})$$

We keep the first- and second-order terms and consider a quasi-neutral hydrogen-electron plasma with $n_H \approx n_e \equiv n$, where the relatively small amount of the lithium is the source of the wave energy. Small concentration of helium is neglected. We can omit the second term in the left-hand side of equation (B2) when calculating the second-order current for the long wavelength daughter waves since $\nabla_{\perp} \equiv ik_{\perp 3} \rightarrow 0$. When $k_{\perp 3}$ is not negligible, then this term may contribute as discussed later. Also, because the mother waves are weakly electromagnetic [see equation (11)], we can neglect $j_{1k_1} B_{1k_2}$ in the right-hand side of equation (B2). This leads to

$$j_x^{(2)} = -\frac{m_H c}{B_0} \frac{\partial}{\partial t} \left(n^{(1)} \vec{v}^{(1)} + n_0 \vec{v}^{(2)} \right)_y. \quad (\text{B3})$$

[51] Now we calculate the ion momentum $(n^{(1)} \vec{v}^{(1)} + n_0 \vec{v}^{(2)})_y / n_0$ with the assumption $k_{\perp 1} + k_{\perp 2} = 0$ and using the normalized quantities, $\omega / \Omega_H \rightarrow \bar{\omega}$, $k_z c / \omega_{pH} \rightarrow \bar{k}_z$, $k_{\perp} c / \omega_{pH} \rightarrow \bar{k}$, $E_x c / B_0 V_A \rightarrow E$, $\vec{v}_{\perp} / V_A \rightarrow \vec{v}$, and $b_0 = \vec{B}_0 / B_0$. In these normalized quantities, the ion motion and density are described by the equations

$$\partial \vec{v} / \partial t = \vec{v} \times \vec{b}_0 + \vec{E} - (\vec{v} \cdot \nabla) \vec{v}, \quad (\text{B4})$$

$$\partial n / \partial t + \nabla_{\parallel} n \vec{v} = 0. \quad (\text{B5})$$

The solution of these equations can be found using expansion over small amplitude of E ,

$$\begin{aligned} \vec{v}_k &= \vec{v}_k^{(1)} + \vec{v}_k^{(2)} \\ &= \frac{\vec{E}_k^{(1)} - \left((\vec{v}^{(1)} \cdot \nabla) \vec{v}^{(1)} \right)_k \times \vec{b}_0 - i \bar{\omega}_k \left(\vec{E}_k^{(1)} - \left((\vec{v}^{(1)} \cdot \nabla) \vec{v}^{(1)} \right)_k \right)}{1 - \bar{\omega}_k^2}, \end{aligned} \quad (\text{B6})$$

$$\vec{v}_k^{(1)} = \frac{\vec{E}_k^{(1)} \times \vec{b}_0 - i \bar{\omega}_k \vec{E}_k^{(1)}}{1 - \bar{\omega}_k^2}, \quad (\text{B7})$$

$$\frac{n_k^{(1)}}{n_0} = \frac{-ikE_k^{(1)}}{1 - \bar{\omega}_k^2}. \quad (\text{B8})$$

In equations (B4)–(B8), the electric field has only x component. Substituting $E^{(1)} = E_{k_1} \exp(-i\omega_{k_1}t + ik_{\perp 1}x + ik_{z1}z) + E_{k_2} \exp(-i\omega_{k_2}t + ik_{\perp 2}x + ik_{z2}z)$ in equation (B4) and keeping only the terms with $k_1 + k_2 = 0$, we get

$$\begin{aligned} \left(\bar{v}^{(1)} n^{(1)} / n_0 \right)_{y k_3} &= \frac{-E_{k_1}}{(1 - \bar{\omega}_{k_1}^2)} \frac{-ik_2 E_{k_2}}{(1 - \bar{\omega}_{k_2}^2)} + \frac{-E_{k_2}}{(1 - \bar{\omega}_{k_2}^2)} \frac{-ik_1 E_{k_1}}{(1 - \bar{\omega}_{k_1}^2)} \\ &= \frac{(k_1 + k_2) E_{k_1} E_{k_2}}{(1 - \bar{\omega}_{k_1}^2)(1 - \bar{\omega}_{k_2}^2)} = 0, \end{aligned} \quad (\text{B9})$$

$$\begin{aligned} \left((\bar{v}^{(1)} \cdot \bar{\nabla}) \bar{v}^{(1)} \right)_{k_3} &= i \left((\bar{v}_{k_1} \cdot \bar{k}_2) \bar{v}_{k_2} + (\bar{v}_{k_2} \cdot \bar{k}_1) \bar{v}_{k_1} \right)_{k_3} \\ &= \frac{-((k_2 \bar{\omega}_{k_1} + k_1 \bar{\omega}_{k_2}) \bar{y} + i \bar{\omega}_{k_1} \bar{\omega}_{k_2} (k_2 + k_1) \bar{x}) E_{k_1} E_{k_2}}{(1 - \bar{\omega}_{k_1}^2)(1 - \bar{\omega}_{k_2}^2)} \\ &= \frac{k_1 (\bar{\omega}_{k_1} - \bar{\omega}_{k_2}) \bar{y} E_{k_1} E_{k_2}}{(1 - \bar{\omega}_{k_1}^2)(1 - \bar{\omega}_{k_2}^2)}, \end{aligned} \quad (\text{B10})$$

and

$$\begin{aligned} j_{y k_3}^{(2)} &= \frac{\left((\bar{v}^{(1)} \cdot \bar{\nabla}) \bar{v}^{(1)} \right)_{x k_3} + i \bar{\omega}_{k_3} \left((\bar{v}^{(1)} \cdot \bar{\nabla}) \bar{v}^{(1)} \right)_{y k_3}}{1 - \bar{\omega}_{k_3}^2} \\ &= -i \frac{k_1 (\bar{\omega}_{k_2} - \bar{\omega}_{k_1}) \bar{\omega}_{k_3} E_{k_1} E_{k_2}}{(1 - \bar{\omega}_{k_3}^2)(1 - \bar{\omega}_{k_1}^2)(1 - \bar{\omega}_{k_2}^2)}. \end{aligned} \quad (\text{B11})$$

Equations (B9)–(B11) lead to

$$\left(n^{(1)} \bar{v}^{(1)} + n_0 \bar{v}^{(2)} \right)_y / n_0 = -i \frac{k_1 (\bar{\omega}_{k_2} - \bar{\omega}_{k_1}) \bar{\omega}_{k_3} E_{k_1} E_{k_2}}{(1 - \bar{\omega}_{k_3}^2)(1 - \bar{\omega}_{k_1}^2)(1 - \bar{\omega}_{k_2}^2)}, \quad (\text{B12})$$

where \bar{x} and \bar{y} are the unit vectors along the x and y directions, respectively. Substituting equation (B12) in equation (B3), we calculate the normalized second-order current,

$$\bar{j}_{x k_3}^{(2)} / en_0 = \frac{k_1 (\bar{\omega}_{k_2} - \bar{\omega}_{k_1}) \bar{\omega}_{k_3}^2 E_{k_1} E_{k_2}}{(1 - \bar{\omega}_{k_3}^2)(1 - \bar{\omega}_{k_1}^2)(1 - \bar{\omega}_{k_2}^2)}. \quad (\text{B13})$$

[52] Equation (24) along with nonlinear current given by equation (B13) can be solved iteratively to obtain $E_x^{(2)}$. Starting with $E_x^{(1)} \equiv E_k$, we solve for the linear frequency ω_3 with $j_x^{(2)} = 0$. Expanding the LHS of equation (24) near the resonant $\omega_{k_3} = \omega_3$, i.e., $(k_{z3}^2 - i\bar{\omega}_{k_3} \sigma_{xx}) \bar{E}_{k_3}^{(2)} \equiv -\bar{D}(\bar{\omega}_{k_3}) \bar{\omega}_{k_3}^2 \bar{E}_{k_3}^{(2)} = -\bar{\omega}_{k_3} (\bar{D}\bar{\omega}_3 + (\bar{\omega}_{k_3} - \bar{\omega}_3) \partial(\bar{D}\bar{\omega}_3)/\partial\bar{\omega}_3) \bar{E}_{k_3}^{(2)} = i\bar{\omega}_{k_3} \bar{j}_{x k_3}^{(2)}$ with $\bar{D}(\omega_3) = 0$ and using equation (B13), we obtain $E_x^{(2)}$,

$$E_{k_3}^{(2)} = -i \frac{(\partial(\bar{D}\bar{\omega}_3)/\partial\bar{\omega}_3)^{-1}}{(\bar{\omega}_{k_3} - \bar{\omega}_3 - i\bar{\gamma})} \frac{k_1 (\bar{\omega}_{k_2} - \bar{\omega}_{k_1}) \bar{\omega}_{k_3}^2 E_{k_1} E_{k_2}}{(1 - \bar{\omega}_{k_3}^2)(1 - \bar{\omega}_{k_1}^2)(1 - \bar{\omega}_{k_2}^2)}. \quad (\text{B14})$$

We introduced a small growth rate γ in order to avoid the singularity at resonance. Also, note that $\bar{D} = -(\bar{k}_z^2/\bar{\omega}_k^2) + 1/(1 - \bar{\omega}_k^2)$ is $D(\omega, k)$ defined in equation (14) in normalized variables.

B2. Rate of Energy Transfer to Daughter Shear Alfvén Waves

[53] Now using $E_{k_3}^{(2)}$ and $j_{k_3}^{(2)}$, we calculate the rate at which the energy is pumped into the newly born daughter wave by the mother wave,

$$\begin{aligned} \left(\frac{d\bar{W}_3}{d(\Omega_H t)} \right)_{2D} &= \bar{j}_{x k_3}^{(2)} E_{k_3}^{* (2)} + c.c. \\ &= \bar{W}_{k_1} \bar{W}_{k_2} \left(k_1 \bar{\omega}_{k_3}^2 (\bar{\omega}_{k_2} - \bar{\omega}_{k_1}) \right)^2 \frac{\bar{\gamma}/2}{(\bar{\omega}_{k_3} - \bar{\omega}_3)^2 + \bar{\gamma}^2}, \end{aligned} \quad (\text{B15})$$

where the wave energy density, $\bar{W}_k = (1/2)|\bar{E}_k|^2 \partial(\bar{D}\bar{\omega}_k)/\partial\bar{\omega}_k \approx |\bar{E}_k|^2/(1 - \bar{\omega}_k^2)^2$, is normalized by $(B_0^2/8\pi)$. We label this rate as two-dimensional because all interacting waves are in one plane. If there is an ensemble of uncorrelated waves (weak turbulence), then the net effect is the sum of the individual interactions. If the resonance condition, i.e., $\omega_{k_1} + \omega_{k_2} = \omega_{k_3}$, $\bar{k}_1 + \bar{k}_2 = \bar{k}_3$, and $\gamma \ll \omega$ is satisfied, then the net effect due to the ensemble is

$$\begin{aligned} \left(\frac{d\bar{W}_3}{d(\Omega_H t)} \right)_{2D} &= \int \int d\vec{k}_1 d\vec{k}_2 k_1^2 \bar{\omega}_{k_3}^4 (\bar{\omega}_{k_2} - \bar{\omega}_{k_1})^2 \\ &\quad \cdot \bar{W}_{k_1} \bar{W}_{k_2} \pi \delta(\bar{\omega}(\vec{k}_3) - \bar{\omega}(\vec{k}_1)) \\ &\quad - \bar{\omega}(\vec{k}_2) \delta(\vec{k}_3 - \vec{k}_1 - \vec{k}_2). \end{aligned} \quad (\text{B16})$$

The wave coalescence rate in equation (B16) cannot be obtained in the usual MHD framework. Also, this rate is strongly dependent on the wave frequency and becomes negligible for $\bar{\omega} \ll 1$. Estimating the integral in equation (B16) under the assumption $\bar{W}_{k_1} \sim \bar{W}_{k_2}$, we obtain the nonlinear rate

$$\left(\frac{d\bar{W}_3}{d(\Omega_H t)} \right)_{2D} \approx (\bar{\omega}_{k_1} + \bar{\omega}_{k_2})^3 (\bar{\omega}_{k_1} - \bar{\omega}_{k_2})^2 \bar{k}_1^2 \bar{W}_1^2. \quad (\text{B17})$$

According to the decay law, equations (18) and (19), we have $\bar{\omega}_{k_1} - \bar{\omega}_{k_2} \approx \bar{\omega}_{k_3}/(\bar{k}_1^2 m_e/m_H)^{1/2}$. Hence

$$\left(\frac{d\bar{W}_3}{d(\Omega_H t)} \right)_{2D} \approx (\bar{\omega}_{k_3}^5 (m_H/m_e) \bar{W}_1^2). \quad (\text{B18})$$

B3. Rate of Energy Transfer to Daughter Magnetosonic Waves

[54] Now we analyze the effects of the spatial derivative term in equation (B2) that was ignored in previous section when we calculated the nonlinear current for the case where all the three waves are in the same plane and $\bar{k}_{\perp 3} = \bar{k}_{\perp 1} + \bar{k}_{\perp 2} = 0$. We estimate the contribution of this term for the case when $\bar{k}_{\perp 3}$ is not negligible and is in the y direction, i.e., not in the (x, z) plane.

[55] This term, $\nabla_y((\bar{E}_{k_1} \times \bar{b}_0)(\bar{E}_{k_2} \times \bar{b}_0))/(1 - \bar{\omega}_{k_1}^2)(1 - \bar{\omega}_{k_2}^2)$, for a small wave vector $\bar{k}_{\perp 3} = \bar{k}_{\perp 1} + \bar{k}_{\perp 2} \ll \bar{k}_{\perp 1}$ out of

the plane (x, z) contributes a nonlinear current, which in the normalized values is

$$\frac{\bar{j}_{xk_3}^{(2)}}{en_0} = \frac{-2i\bar{k}_{y3}(E_{xk_1}E_{xk_2})}{(1 - \bar{\omega}_{k_1}^2)(1 - \bar{\omega}_{k_2}^2)}. \quad (\text{B19})$$

The wave vector k_{y3} and nonlinear current $j_{xk_3}^{(2)}$, which is proportional to k_{y3} , correspond to the magnetosonic daughter wave. Similar procedure as above leads to the estimate of the pump rate of the short wavelength mother shear Alfvén waves into the long wavelength magnetosonic daughter waves with $k_{y3} \sim \omega_{pi}/c$,

$$\begin{aligned} \left(\frac{d}{d(\Omega_1 t)} \bar{W}_{k_3} \right)_{3D} &= \bar{j}_{xk_3}^{(2)} E_{k_3}^{*(2)} + c.c. \\ &= \frac{\bar{W}_{k_1} \bar{W}_{k_2} k_{y3}^2}{(\partial(\bar{D}_{MS} \bar{\omega}_{k_3}) / \partial \bar{\omega}_{k_3})} \frac{\bar{\gamma}}{(\bar{\omega}_{k_3} - \bar{\omega}_{MS}(\bar{k}_3))^2 + \bar{\gamma}^2}, \end{aligned} \quad (\text{B20})$$

where $\bar{D}_{MS} = 1 - \bar{k}_{y3}^2 / \bar{\omega}_{k_3}^2$ is the normalized dispersion relation for the magnetosonic daughter waves. For an ensemble of such uncorrelated waves, we estimate the pump rate into the long wavelength magnetosonic daughter waves to be

$$\left(\frac{d}{d(\Omega_1 t)} \bar{W}_{k_3} \right)_{3D} \approx \bar{\omega}_{k_3} \bar{W}_{k_1}^2. \quad (\text{B21})$$

B4. A Physical Explanation of the Origin of the Second-Order Current

[56] In calculating the second-order current, we Fourier-transformed the quantities, and in the process, some clarity of physics was sacrificed. To illustrate the physics of the origin of the second-order current, now we calculate this current without resorting to Fourier transform. However, to simplify the calculation, we will assume low frequency, i.e., $\omega \ll \Omega_H$ so that $1 - \bar{\omega}^2 \approx 1$. The nonlinear current is driven by the rate of temporal change of the plasma momentum given by equation (B12). In terms of the mother wave electric fields, the nonlinear force is given by

$$-Mn_0 \left(\left(\frac{c\vec{E} \times \vec{b}}{B_0} + \frac{\partial}{\partial t} \left(\frac{c\vec{E}}{B_0} \right) \right) \cdot \vec{\nabla} \right) \left(\frac{c\vec{E} \times \vec{b}}{B_0} + \frac{\partial}{\partial t} \left(\frac{c\vec{E}}{B_0} \right) \right). \quad (\text{B22})$$

We assume that all the interacting waves are in one plane, the (x, z) plane, and note that the spatial derivative on a second-order quantity is proportional to k_3 and hence negligible. Hence the nonlinear force (B22) in this plane becomes

$$-Mn_0 \left(\frac{\partial}{\partial t} \left(\frac{c\vec{E}}{B_0} \right) \cdot \vec{\nabla} \right) \frac{c\vec{E} \times \vec{b}}{B_0}, \quad (\text{B23})$$

and leads to the second-order ion inertial drift and momentum,

$$-Mn_0 \frac{\partial}{\partial t} \left[\left(\frac{\partial}{\partial t} \left(\frac{c\vec{E}}{B_0} \right) \cdot \vec{\nabla} \right) \left(\frac{c\vec{E} \times \vec{b}}{B_0} \right) \right]. \quad (\text{B24})$$

The rate of temporal change of this momentum induces the nonlinear current [equation (B2)],

$$\bar{j}^{(2)} = -en_0 \frac{\partial^2}{\Omega^3 \partial t^2} \left[\left(\frac{\partial}{\partial t} \left(\frac{c\vec{E}}{B_0} \right) \cdot \vec{\nabla} \right) \left(\frac{c\vec{E}}{B_0} \right) \right] \quad (\text{B25})$$

Consider the superposition of two waves, for example, mother shear Alfvén waves: $E_x = E_{k_1} \sin(\omega_{k_1} t - k_{z1} z - k_1 x) + E_{k_2} \sin(\omega_{k_2} t + k_{z2} z + k_1 x)$. Substituting this E_x in equation (B25), we get

$$\begin{aligned} j_x^{(2)} &= -en_0 \frac{c^2 E_{k_1} E_{k_2} k_1 (\omega_{k_1} - \omega_{k_2})}{\Omega^4 B_0^2} \frac{\partial^2}{\partial t^2} \\ &\quad [\cos((\omega_{k_1} + \omega_{k_2})t - (k_{z1} - k_{z2})z) \\ &\quad + \cos((\omega_{k_1} - \omega_{k_2})t - (k_{z1} + k_{z2})z - 2k_1 x)] \end{aligned} \quad (\text{B26})$$

The induced long wavelength (averaged over x) nonlinear current is

$$j_x^{(2)}/en_0 = \frac{k_1 (\omega_{k_2} - \omega_{k_1}) \omega_{k_3}^2}{\Omega^4} \frac{c^2 E_{k_1} E_{k_2}}{B_0^2} \cos(\omega_{k_3} t - (k_{z1} - k_{z2})z) \quad (\text{B27})$$

This current due to superposition of two short wavelength mother waves being in resonance, i.e., $\omega_{k_1} + \omega_{k_2} = \omega_{k_3}$, $k_{z1} - k_{z2} = k_{z3}$, gives rise to the long wavelength daughter shear Alfvén wave. In normalized values and in Fourier representation, it is identical to that in equation (B13).

Appendix C: Production of Neutral Clouds by Impact

[57] It is found that approximately 9 kg of Ti/2B is necessary to vaporize 1 kg of lithium (P. Zavitsanos, private communication). This implies that a total mass of 10 tons must be transported into the orbit. Proven technology can accomplish this, but arguably, there is advantage in increasing the energy yield for the same mass. Hence we suggest utilization of the orbital kinetic energy of the lithium itself for vaporization. To exploit this, we note that the specific evaporation heat decreases as pressure increases. At pressure and temperature over 680 atmospheric pressure and 3200 K, respectively, the specific evaporation heat reduces to zero. In such a high-pressure environment, the energy supplied will be directly converted into the lithium internal energy. Such a condition arises in an asteroid-planet impact and may be replicated by colliding a lithium mass (a flux of lithium granules) moving with the satellite velocity $V_s \sim 7$ km/s with a heavy target moving in the opposite direction with the same velocity. At collision, the solid lithium will be converted into a hot lithium vapor expanding with an average velocity larger than V_s depending on the lithium and target mass ratio. As the neutral gas expands with high speed, it will rapidly cool down, and a lithium cloud will be formed. The process of condensation, which could lead to the formation of debris, depends strongly on the impact velocity and vapor density and can be avoided by designing the lithium granule flux to be sufficiently low [Zel'dovich and Raizer, 2002].

[58] For example, consider the collision of a granular lithium mass of 2.5 tons with an aluminum slab of the surface area 30 m² and a mass of 7.5 tons used as the heavy target. These masses could be directed against one another in Keplerian orbit in the equatorial plane for a controlled

collision in the region of interest. The impact will raise the pressure in lithium vapor up to a million times the atmospheric level, and the orbital kinetic energy will be converted into the internal energy of the materials involved. With this internal energy, the lithium gas will expand with an average velocity $\sim V_s + 2V_{cm}$, where V_{cm} is the center of mass velocity of the colliding system. This corresponds to an average energy of approximately 7 eV per atom. The resulting neutral lithium cloud will expand in the equatorial plane mostly outward under the influence of increased centrifugal force since gas expansion in vacuum proceeds with different velocity for different fluid element. Away from the impact region, this expansion will create a moving thin sheet of neutral lithium atoms, which will photoionize into a lithium plasma and seed the electromagnetic turbulence in the way we described earlier. However, the power (~ 100 MW) and energy (~ 300 GJ) released in this case are an order-of-magnitude larger because the energy of the injected lithium atoms is much larger. Thus with same mass transported into the orbit, it may be possible to deliver about an order-of-magnitude more energy and power by the impact vaporization method. This obviously is the major advantage of this method. However, the technology involved in the impact vaporization is not fully matured and will require fine-tuning.

[59] The collision will also vaporize the aluminum. Because of conservation of momentum and energy during the impact of light lithium mass with the heavy aluminum target, the aluminum atoms will lose energy, while the lithium atoms will gain energy. Consequently, the aluminum atoms will slow down and fall earthward because of the action of gravity leaving behind the lithium atoms to photoionize and form a ring distribution and generating intense electromagnetic turbulence as discussed in the text.

[60] **Acknowledgments.** Discussion with P. Zavitsanos regarding neutral release is acknowledged. This work is supported by ONR and DARPA.

[61] Amitava Bhattacharjee thanks the reviewers for their assistance in evaluating this paper.

References

- Bernhardt, P. A. (1992), Probing the magnetosphere using chemical releases from the Combined Release and Radiation Effects Satellite, *Phys. Fluids B*, 4, 2249.
- Bernhardt, P. A., and M. P. Sulzer (2004), Incoherent scatter measurements of ring-ion beam distributions produced by space shuttle exhaust injections into the ionosphere, *J. Geophys. Res.*, 109, A02303, doi:10.1029/2002JA009693.
- Bernhardt, P. A., J. D. Huba, W. E. Swartz, and M. C. Kelley (1998), Incoherent scatter from space shuttle and rocket plumes in the ionosphere, *J. Geophys. Res.*, 103, 2239.
- Brice, N. (1970), Artificial enhancement of energetic particle precipitation through cold plasma injection, *J. Geophys. Res.*, 75, 4890.
- Brice, N., and C. Lucas (1971), Influence of magnetospheric convection and polar wind loss of electrons from the outer radiation belt, *J. Geophys. Res.*, 76, 900.
- Craven, P. D., D. L. Gallagher, and R. H. Comfort (1997), Relative He⁺ in the inner magnetosphere as observed by the DE 1 retarding ion mass spectrometer, *J. Geophys. Res.*, 102, 2279.
- Cuperman, S., and R. W. Landau (1974), On the enhancement of the whistler mode instability in magnetosphere by cold plasma injection, *J. Geophys. Res.*, 79, 128.
- Galeev, A. A., and R. Z. Sagdeev (1988), Alfvén waves in a space plasma and its role in the solar wind interaction with comets, *Astrophys. Space Sci.*, 144, 427.
- Ganguli, G., P. Palmadesso, and J. Fedder (1984), Temporal evolution of whistler growth in a cold plasma injection experiment, *J. Geophys. Res.*, 89, 7351.
- Ganguli, G., and L. Rudakov (2004), Rotation waves in a multi-component plasma, *Phys. Rev. Lett.*, 93, 135001.
- Ganguli, G., and L. Rudakov (2005), Magnetodynamics of a multicomponent (dusty) plasma. I. Rotation waves near low-frequency cutoff in a homogeneous medium, *Phys. Plasmas*, 12, 042110.
- Giles, B. L., M. A. McCook, M. W. McCook, and G. P. Miller (1995), CRRES Combined Radiation and Release Effects Satellite Program, *NASA Technical Memorandum 108494*.
- Hargreaves, J. K. (1992), in *The Solar-Terrestrial Environment: An Introduction to Geospace*, edited by J. T. Houghton, M. J. Rycroft, and A. J. Dessler, p. 178, Cambridge Univ. Press, New York.
- Hizanidis, K., P. J. Cargill, and K. Papadopoulos (1988), Lower hybrid waves upstream of comets and their implications for the comet Halley "Bow Wave", *J. Geophys. Res.*, 93, 9577.
- Inan, U. S., T. F. Bell, J. Bortnik, and J. M. Albert (2003), Controlled precipitation of radiation belt electrons, *J. Geophys. Res.*, 108(A5), 1186, doi:10.1029/2002JA009580.
- Kennel, C. F., and H. E. Petschek (1966), Limit on stably trapped particles, *J. Geophys. Res.*, 71, 1.
- Lyons, L. R., R. M. Thorne, and C. F. Kennel (1971), Electron pitch-angle diffusion driven by oblique whistler-mode turbulence, *J. Plasma Phys.*, 6, 589.
- Lyons, L. R., R. M. Thorne, and C. F. Kennel (1972), Pitch-angle diffusion of radiation belt electrons within plasmasphere, *J. Geophys. Res.*, 77, 3455.
- Lyons, L. R. (1974), Pitch angle and energy diffusion coefficients from resonant interactions with ion-cyclotron and whistler waves, *J. Plasma Physics*, 12, 417.
- McClements, K. G., R. O. Dendy, and C. N. Lashmore-Davies (1994), A model for the generation of obliquely propagating ULF waves near the magnetic equator, *J. Geophys. Res.*, 99, 23,685.
- Meredith, N. P., M. Cain, R. B. Horne, R. M. Thorne, D. Summers, and R. R. Anderson (2003), Evidence for chorus-driven electron acceleration to relativistic energies from a survey of geomagnetically disturbed periods, *J. Geophys. Res.*, 108(A6), 1248, doi:10.1029/2002JA009764.
- Mikhailovskii, A. B., E. A. Novakovskaya, V. P. Lakhin, S. V. Novakovskii, O. G. Onishchenko, and A. I. Smolyakov (1989), Contribution to the theory of weakly turbulent Kolmogorov spectra of a homogeneous magnetized plasma, *Sov. Phys. JETP, Engl. Transl.*, 68, 924.
- Onishchenko, O. G., O. A. Pokhotelov, R. Z. Sagdeev, L. Stenflo, V. P. Pavlenko, P. K. Shukla, and V. V. Zolotukhin (2003), Modification of Kolmogorov spectra of weakly turbulent shear Alfvén waves by dust grains, *Phys. Plasmas*, 10, 69.
- Rauch, J. L., and A. Roux (1982), Ray tracing of ULF waves in a multi-component magnetospheric plasma: Consequences for the generation mechanism of ion cyclotron waves, *J. Geophys. Res.*, 87, 8191.
- Roux, A., S. Perraut, C. de Villedary, A. Korth, G. Kremser, J. L. Rauch, and D. T. Young (1984), Propagation and amplification of ICW's in a multicomponent plasma. The earth magnetosphere as a giant maser for Alfvén waves, in *ESA Achievements of the Intern. Magnetospheric Study (IMS)*, p. 589 (SEE N85-24544 14-46).
- Rudakov, L., and G. Ganguli (2005), Magnetodynamics of a multicomponent (dusty) plasma: II. Magnetic drift waves in an inhomogeneous medium, *Phys. Plasmas*, 12, 042111.
- Shapiro, V. D., V. I. Shevchenko, A. S. Sharma, K. Papadopoulos, R. Z. Sagdeev, and V. B. Lebedev (1993), Lower hybrid turbulence at cometary bow wave and acceleration of cometary protons, *J. Geophys. Res.*, 98, 1325.
- Sharma, O. P., and V. L. Patel (1986), Low-frequency waves driven by gyrotropic gyrating ion beams, *J. Geophys. Res.*, 91, 1529.
- Shukla, P. K., and L. Stenflo (2005), Decay of a magnetic-field-aligned Alfvén wave into inertial and kinetic Alfvén waves in plasmas, *Phys. Plasmas*, 12, 084502.
- Stix, T. H. (1992), in *Waves in Plasmas*, p. 342, American Institute of Physics, New York.
- Summers, D., and R. M. Thorne (2003), Relativistic electron pitch angle scattering by electromagnetic ion cyclotron waves during geomagnetic storms, *J. Geophys. Res.*, 108(A4), 1143, doi:10.1029/2002JA009489.
- Summers, D., R. M. Thorne, and F. Xiao (1998), Relativistic theory of wave-particle resonant diffusion with application to electron acceleration in the magnetosphere, *J. Geophys. Res.*, 103, 20,487.
- Voitenko, Y., and M. Goossens (2005), Cross-scale nonlinear coupling and plasma energization by Alfvén waves, *Phys. Rev. Lett.*, 94, 135003.
- Zel'dovich, Ya. B. and Yu. P. Raizer (2002), in *Physics of Shock Waves And High-Temperature Hydrodynamic Phenomenon*, edited by W. D. Hayes and R. F. Probstein, Chaps. VIII, XI, and XII, Dover, Mineola, N. Y.

G. Ganguli, Plasma Physics Division, Naval Research Laboratory, Washington, DC 20375, USA. (gang@ppd.nrl.navy.mil)

M. Mithaiwala, National Research Council, Naval Research Laboratory, Washington, DC, USA.

K. Papadopoulos, Department of Physics and Astronomy, University of Maryland, College Park, MD 20742, USA.

L. Rudakov, Icarus Research Inc., P.O. Box 30780, Bethesda, MD 20824-0780, USA.